Palaeobiogeographical distribution of Smithian (Early Triassic) ammonoid faunas within the western USA basin and its controlling parameters.

Romain Jattiot, Arnaud Brayard, Hugo Bucher, Emmanuelle Vennin, Gwénaël Caravaca, James F. Jenks, Kevin G. Bylund, Gilles Escarguel

PALAEOBIOGEOGRAPHICAL STRUCTURATION OF SMITHIAN (EARLY TRIASSIC) AMMONOID FAUNAS WITHIN THE WESTERN USA BASIN AND ITS CONTROLLING PARAMETERS

Published *in* Palaeontology 61, 881-904

by ROMAIN JATTIOT[1, 2], ARNAUD BRAYARD[2], HUGO BUCHER[1], EMMANUELLE VENNIN[2], GWÉNAËL CARAVACA[2], JAMES F. JENKS[3], KEVIN G. BYLUND[4] *and* GILLES ESCARGUEL[5]

[1]Paläontologisches Institut der Universität Zürich, Karl Schmid-Strasse 4, 8006, Zürich, Switzerland; e-mail: romain.jattiot@pim.uzh.ch

[2]Biogéosciences, UMR 6282, CNRS, Université Bourgogne Franche-Comté, 6 boulevard Gabriel, 21000 Dijon, France

[3]1134 Johnson Ridge Lane, West Jordan, Utah 84084, United States of America

[4]140 South 700 East, Spanish Fork, Utah 84660, United States of America

[5]Univ. Lyon, Université Claude Bernard Lyon 1, CNRS, ENTPE, UMR 5023 Laboratoire d'Ecologie des Hydrosystèmes Naturels et Anthropisés, 27-43 boulevard du 11 novembre 1918, 69622 Villeurbanne Cedex, France

Abstract: We present the first quantitative palaeobiogeographical analysis in terms of distribution and abundance of Early Triassic ammonoids from the western USA basin during the Smithian, ca. 1 myr after the Permian-Triassic boundary mass extinction. The faunal dataset consists of a taxonomically homogenized compilation of spatial and temporal occurrences and abundances from 39 sections distributed within the western USA basin. Two complementary multivariate techniques were applied to identify the main biogeographical structuring recorded in the analysed presence/absence data: additive Cluster Analysis using the Neighbor-Joining algorithm (NJ) and Non-metric Multidimensional Scaling (NMDS). Regarding abundance data, a taxonomic diversity (*sensu* evenness) analysis was coupled with graphical comparisons of relative abundances of selected taxa. The identified relationships indicate that middle Smithian ammonoids of the western USA basin were geographically organized in terms of both distribution and abundance, with the

biogeographical distinction of a southern and a northern cluster. This N/S structuring in the distribution and abundance of middle Smithian ammonoids is notably paralleled by the relative amount of siliciclastics, which suggests that clastic load of the water column and possibly salinity were among the main controlling factors. In marked contrast with the middle Smithian, the studied late Smithian ammonoid assemblages do not show any significant difference, whatever the depositional environments. This abrupt biogeographical homogenization independent from intrabasinal facies heterogeneity indicates a switch from regional to global drivers, associated with the well-known late Smithian global extinction and remarkable cosmopolitan ammonoid distributions during that time.

Key words: Early Triassic, ammonoids, palaeobiogeography, distribution, abundance, depositional environments.

FOLLOWING the Permian-Triassic boundary mass extinction (PTBME), the Early Triassic is commonly interpreted to be a highly perturbed ~5 myr time interval, as recorded by globally documented fluctuations of the carbon cycle (e.g., Payne *et al*. 2004; Galfetti *et al*. 2007) and oxygen isotopes (e.g., Romano *et al*. 2013). Nevertheless, nekto-pelagic organisms such as ammonoids recovered very quickly in comparison with many other marine organisms, reaching diversity levels much higher than during the Permian already in the Smithian, ca. 1 myr after the PTBME (Brayard *et al*. 2009*a*; Zakharov & Abnavi 2013; Zakharov & Popov 2014; Brayard & Bucher 2015). In this context, the Smithian is a crucial ~0.7 myr long interval recording the first major, global ammonoid diversification-extinction cycle after the PTBME (Fig. 1). Indeed, the main rediversification of ammonoids occurred during the early and middle Smithian (e.g., Brayard *et al*. 2006, 2009*a*; Brühwiler *et al*. 2010*a*; Ware *et al*. 2015), whereas the most severe intra-Triassic crisis for the nekton took place in the late Smithian (Tozer 1982; Hallam 1996; Brühwiler *et al*. 2010*a*; Jattiot *et al*. 2016; Fig. 1). This major late Smithian event, preceded by a middle Smithian C-isotope negative peak and a spore spike (e.g., Hermann *et al*. 2011), was concomitant with: (1) a shift from latitudinally-constrained to cosmopolitan ammonoid distributions (Tozer 1982; Dagys 1988; Brayard *et al*. 2006); (2) the transient loss of sphaerocone ammonoids (Brosse *et al*. 2013); (3) the onset of a global positive shift of the carbon cycle (Galfetti *et al*. 2007; Fig. 1); and (4) a quick ecological recovery of

gymnosperms (Hermann *et al*. 2011). Overall, these events indicate the occurrence of major successive and global environmental changes during the Smithian.

Smithian ammonoid assemblages have been recently revised worldwide (e.g., western USA: Brayard *et al*. 2009*b*, 2013; Jenks *et al*. 2010; Stephen *et al*. 2010; Jattiot *et al*. 2017; Guangxi: Brayard & Bucher 2008; South Primorye: Zakharov *et al*. 2002; Shigeta & Zakharov 2009; Shigeta *et al*. 2009; Zakharov *et al*. 2013; Shigeta & Kumagae 2015; South Tibet: Brühwiler *et al*. 2010*b*; Oman: Brühwiler *et al*. 2012*a*; Salt Range: Brühwiler *et al*. 2012*b*; Spiti: Brühwiler *et al*. 2012*c*; Vietnam: Shigeta & Nguyen 2014; Fig. 2), and their biogeographical affinities have been examined at a global scale (Brayard *et al*. 2006, 2007, 2009*c*, 2015).

In this work, we quantitatively investigate the biogeography of Smithian ammonoids within the western USA basin, i.e., at a regional scale finer than all Early Triassic biogeographical ammonoid studies conducted so far. We discuss the potential parameters controlling the distribution and abundance of ammonoid faunas at this mesoscale. Various relationships between ammonoid shell morphologies and particular lifestyles have already been hypothesized in the literature (e.g., Raup & Chamberlain 1967; Swan & Saunders 1987; Jacobs 1992; Batt 1993; Wang & Westermann 1993; Jacobs *et al*. 1994; Westermann 1996; Klug & Korn 2004; Monnet *et al*. 2011); and variations of morph frequencies have classically been related to taphonomic and environmental fluctuations within a basin (e.g., distinct habitats, bathymetry, salinity, terrigenous inputs and oceanic currents; e.g., Company 1987; Bulot 1993). In some examples, a link was suggested between the type of sediment and shell compression and involution (Bayer & McGhee 1984; Saunders & Swan 1984; Batt 1989; Jacobs *et al*. 1994; Westermann 1996; Neige *et al*. 1997; Klug 2002; Kawabe 2003; Wani 2003). For instance, within a restricted oceanic basin (e.g., Kawabe 2003), compressed forms are sometimes more frequently associated with high-energy, sandy facies (e.g., nearshore), whereas depressed morphs predominate within low-energy, mud-dominated facies (e.g., offshore). Here, we explore such relationships and their potential underlying controls within a single basin benefiting from a robust biochronological frame. This regional mesoscale approach, classically referred to as γ-diversity, is seen as an indispensable step that may help sorting out palaeobiogeographical analyses and interpretations when moving up at the global geographical scale within a highly resolved temporal frame.

GEOLOGICAL SETTING

The western USA basin was located at a near-equatorial position in eastern Panthalassa during the Early Triassic (Fig. 2), and was interpreted as a foreland basin related to the emplacement of the Golconda Allochthon during the Sonoma orogeny (e.g., McKee 1954; Collinson *et al*. 1976; Caravaca *et al*. in press). Early Triassic epicontinental marine strata of the Thaynes Group (*sensu* Lucas *et al*. 2007) were deposited over a large area including Nevada, Utah, Idaho, southern Montana and western Wyoming. The maximum onlap of the Thaynes Group occurred during the late Smithian (Collinson & Hasenmueller 1978; Carr & Paull 1983; Paull & Paull 1993; Lucas *et al*. 2007). The relative positions of the studied sections within the basin have not been significantly altered since the Early Triassic, although the basin underwent successive compressive and extensive tectonic constraints (e.g., Caravaca *et al*. in press). During the Early Triassic, studied sections were located slightly more westward compared to their respective present-day position (see next section).

Although lateral facies changes in the basin have been documented since the beginning of the 20th century (e.g., Gilluly & Reeside 1927; Mansfield & Girty 1927; McKee 1954), Caravaca *et al*. (in press) provided a very detailed account on lithologies, thickness, and subsidence rates. A distinction between the northern part (including southeastern Idaho) and the southern part (including central and southern Utah) of the basin has long been noticed and was recently interpreted as the influence of rheological properties of the basement terranes and spatial heterogeneity of the Golconda Allochthon (Caravaca *et al*. in press).

This N/S differentiation is also empirically perceptible in the distribution of middle Smithian faunas within the basin, some occurrences being apparently restricted to a single sub-basin and/or relative frequencies being highly disparate. This is particularly pronounced for ammonoids, but such a biogeographical pattern still needs to be quantitatively investigated based on a large dataset covering the entire basin and the largest possible array of depositional settings.

The taxonomy and biostratigraphy of Smithian ammonoids from this basin also benefits from recent and thorough treatments (Brayard *et al*. 2013; Jattiot *et al*. 2016, 2017). Comprehensive stratigraphical successions yielding faunal sequences are essentially found in the southern and southwestern part of the basin, whereas sections in the northern part rarely yield more than two faunas of Smithian age. These primary

biostratigraphical data have been processed quantitatively by means of the Unitary Associations method, providing a robust time frame for the basin (Jattiot *et al*. 2017).

DATA AND METHODS

Nature of the dataset

The original dataset consists of a taxonomically homogenized compilation of ammonoid occurrence and abundance of 19 early Smithian taxa, 73 middle Smithian taxa, and 13 late Smithian taxa in 39 sections within the western USA basin. Palaeopositions of these sections were reconstructed based on the retrodeformation scheme of Caravaca *et al*. (in press; Fig. 3). Sections providing early Smithian data (Brayard *et al*. 2013; Jattiot *et al*. 2017) are too few for an adequate geographical coverage and these were consequently discarded. Hence, the present analyses focus on middle and late Smithian data, which correspond to two time subdivisions (UAZ_4 and UAZ_{5+6}, respectively, as defined by Jattiot *et al*. 2017).

Some taxa were not identified at the species level, either because of poor preservation or because of still unresolved taxonomy as exemplified by *Juvenites*. Uniques, i.e., taxa found in only one section, are an important part of the initial middle Smithian dataset (40 out of 73 taxa, i.e., 55 %), and 31 % of the late Smithian dataset (4 out of 13 taxa). Because the spatial distribution of uniques strongly depends on differential sampling effort at the local scale, these were removed from the analysed dataset. Sections suffering from insufficient sampling effort resulting simultaneously in low specimen numbers and low taxonomic richness were also removed. Hence, the results presented and discussed in this paper are based on the numerical analysis of the final middle (UAZ_4) and late Smithian (UAZ_{5+6}) dataset, including 33 taxa in 20 sections and 9 taxa in 7 sections, respectively.

Hierarchical clustering and ordination analyses of presence/absence data

Two complementary multivariate techniques were applied using PAST 3.14 (Hammer *et al*. 2001) to identify the main biogeographical structuring recorded in the analysed datasets: additive Cluster Analysis using the Neighbor-Joining algorithm (NJ) and 2D Non-metric Multidimensional Scaling (NMDS) (Legendre & Legendre 2012). Both

170 analyses are based on the preliminary computation of the same similarity matrix,
171 using the Dice (or Sørensen) index for presence/absence data (S_{Dice}; see Brayard *et al.*
172 2007, 2015 and Peybernes *et al.* 2016 for the justification of such choice; basic
173 properties of other indices can be found in, e.g., Koleff *et al.* 2003). A comparison
174 and combination of results obtained with hierarchical clustering and NMDS improve
175 the description and reinforce the confidence in the recognized biogeographical
176 structures (e.g., Sneath & Sokal 1973; Field *et al*. 1982; Brayard *et al*. 2007; Legendre
177 & Legendre 2012). The minimum spanning tree (chain of primary connections;
178 Kruskal 1956; Prim 1957) associated with the analysed similarity matrix was
179 superimposed onto the NMDS map, whose Kruskal's stress value is given. A high
180 stress value reflects a poor representation of the taxonomic similarities between
181 assemblages by the NMDS map (Legendre & Legendre 2012).
182 To further decipher the biogeographical structuring identified through NJ and NMDS
183 analyses, a (one-way) ANOSIM test coupled with a SIMPER analysis (both using
184 S_{Dice}) was also performed using PAST 3.14 (Hammer *et al*. 2001). The ANOSIM test
185 is a non-parametric, permutation-based procedure testing the null hypothesis of
186 random compositional differences between sample groups (Clarke 1993). Rejection of
187 the null hypothesis involves that sample groups are "real", i.e., groups show non-
188 randomly different taxonomic compositions based on within-group compositional
189 variability. When the ANOSIM test returns a significant difference among groups, a
190 SIMPER analysis can be performed to identify the taxa driving the between-group
191 differences (Clarke 1993). By identifying what taxa are mainly contributing to the
192 compositional differences between sample groups, results from the SIMPER analysis
193 help in the taxonomical characterization of the biogeographical clusters (Brayard *et*
194 *al*. 2015).
195 When using the Dice similarity index, localities with close taxonomic richness may
196 cluster together, potentially preventing to determine whether this grouping is a
197 genuine compositional (i.e., biogeographic) signal or results from a taxonomic
198 richness-induced bias unrelated with the biogeographical history of the studied
199 assemblages (Baselga 2010, 2012). To complement our analyses and to untangle the
200 potential effect of taxonomic richness and composition on the NJ and NMDS
201 analyses, we additively decomposed the 1-complement of the Dice similarity matrix,
202 $D_{dice} = 1\text{-}S_{dice}$, into two independent components: a turnover-component dissimilarity

matrix known as the Simpson dissimilarity matrix (D_{Simp} with $D_{Simp} = \frac{C}{\min(A,B)}$; Simpson, 1960, where *A* and *B* are the number of taxa in samples *A* and *B*, and *C* is the number of taxa shared by *A* and *B*), and a nestedness-resultant component dissimilarity matrix referred to as the Nestedness dissimilarity matrix where $D_{nest} = D_{dice} - D_{simp}$ (Baselga 2010, 2012). The comparison of D_{dice} ("total" taxonomical dissimilarity), D_{simp} (compositional dissimilarity), and D_{nest} (richness dissimilarity) using one-tailed Mantel tests (9,999 permutations) allows the separate effect of richness (Nestedness) and compositional (Simpson) dissimilarities on the "total" (Dice) taxonomic dissimilarity to be assessed.

Taxonomic diversity based on abundance data

A taxonomic diversity analysis was performed using the one-complement of Simpson's (1949) index $D = \sum_{i=1}^{i=N} p_i^2$, i.e., the commonly called Simpson's Index of Diversity, with *N* = the number of taxa sampled in a given assemblage and $p_i = \frac{n_i}{M}$ where n_i = the number of specimens sampled for taxon *i* and *M* = the total number of specimens in a given assemblage. Under random sampling conditions, 1 – *D* (ranging between 0 and 1) is an unbiased estimate of the probability that two specimens randomly drawn from an assemblage belong to two different taxa (also known as the *probability of interspecific encounter*; Hurlbert 1971). On that ground, 1 – *D* measures the diversity (*sensu* evenness) of a taxonomic assemblage: the higher 1 – *D*, the more equable the abundances of the taxa in the assemblage. The index 1 – *D* was computed (using PAST 3.14; Hammer *et al*. 2001) based on 11 taxa selected for their high average relative abundance and highly significant χ^2 test for contingency table (Sokal & Rohlf 1995; Table 1) within 15 middle Smithian sections, each showing at least *M* = 90 identified specimens (this limit was chosen for the sake of sample representativeness, based on the graphical identification of a threshold in the M-distribution around this value; Table 1 in Supplementary Data). The same 11 taxa were finally used for graphical comparisons of their relative abundances based on 95% 'exact' (i.e., using Clopper-Pearson method) confidence intervals on empirical proportions (also using PAST 3.14; Hammer *et al*. 2001).

Depositional environments

Table 2 summarizes the main ammonoid-rich facies labelled A, B, C and D (Fig. 4) and their corresponding depositional environments that were identified in the 15 middle Smithian sections selected for taxonomic diversity analyses (see above). Identification of these facies by means of petrographic analyses was conducted both macroscopically and microscopically on thin sections and polished slabs. Thin sections have been analysed with optical polarizing microscope. Sections are labelled according to their facies in the appropriate figures. Some sections yielded several fossiliferous middle Smithian beds and therefore, might include more than one depositional environment (e.g., Stewart Canyon). Noteworthy, southern sections and Palomino Ridge share the same facies (facies A), which is not found elsewhere in the basin. This facies, corresponding to the deepest environment, is also singularly characterized by the presence of siltstones (Table 2), indicative of a mixed siliciclastic-carbonate regime.

RESULTS

Middle Smithian

Geographical structuring of taxonomic assemblages based on presence/absence data. The Neighbour Joining tree (Fig. 5A) allows the identification of three geographically consistent clusters: mSm1, containing all northern (Idaho) sections plus the Nevada section CS 23; mSm2, grouping the Nevada sections Crittenden Springs and Palomino Ridge; and mSm3, corresponding to the four southern (Utah) sections. Therefore, the NJ tree's topology suggests that the northern and southern parts of the basin differ in terms of faunal assemblages, with mSm2 sections appearing closer to southern ones in terms of taxonomical composition. WIL 9/14 occupies an intermediate position between mSm1 and the mSm2/mSm3 group. Noteworthy, in spite of its geographical proximity with mSm2 (Fig. 3A), CS 23 clusters with mSm1 sections.

The NMDS analysis (Fig. 5B) returns a biogeographical structuring compatible with the NJ tree, with mSm3 being well separated from mSm1, suggesting that southern and northern parts of the basin are distinct from each other in their ammonoid assemblages. On the one hand, the three Nevada sections Palomino Ridge, Crittenden Springs and WIL 9/14 form a distinct intermediate group between mSm1 and mSm3.

WIL 9/14 is compositionally closer to mSm1, Palomino Ridge closer to mSm3, and Crittenden Springs falls in between. Therefore, we expand the composition of mSm2 as defined in the NJ tree by now clustering those three Nevada sections in the NMDS (Fig. 5B). On the other hand, as already shown by the NJ tree, CS 23 appears more similar to mSm1 assemblages than to the three mSm2 sections.

Mantel tests between D_{Dice}, D_{Simp} and D_{Nest} (see Data and Method section) show a strong and highly significant positive linear correlation between the Dice ("total") and Simpson (compositional) dissimilarity matrices ($R = 0.682$; $p \leq 0.00001$). On the other hand, the Dice and Nestedness (richness) dissimilarity matrices show a weak but slightly significant positive correlation ($R = 0.195$; $p = 0.02$), suggesting that a few similarities among assemblages based on the Dice coefficient may be affected by differences in taxonomic richness, and thus may not properly reflect richness-free variations of taxonomic composition. Nevertheless, these potentially artefactual clusters are easy to identify and do not preclude the existence of clusters mSm1, mSm2 and mSm3: two are intra-mSm3 and discriminate localities with high (Confusion Range-Pahvant Range) *vs*. low (Mineral Mountains-Torrey area) taxonomic richness (Fig. 5A). Another cluster groups the Schmid Ridge, The Pond and 2S assemblages from mSm1; these three localities show a high taxonomic richness, but this cluster is well supported in terms of composition as it corresponds to geographically very close sample localities with occurrences of relatively endemic taxa (e.g., *Wyomingites*; see next sections). Overall, the main, three-group structuring identified through NJ and NMDS analyses of the Dice similarity matrix thus appears as a genuine biogeographical signal unbiased by taxonomic-richness differences among the studied assemblages.

This three-group structuring is corroborated by the (one-way) ANOSIM test of the Dice similarity matrix, which demonstrates a significant overall compositional difference among the three clusters ($R = 0.54$, $p = 0.0003$) driven by the strong compositional difference between mSm1 and mSm3 (Table 2 in Supplementary Data). The intermediate position of mSm2 is also confirmed, since it is only marginally to non-significantly distinct from the southern and northern clusters.

Based on these results and to further evaluate the gradational interpretation of mSm2 between mSm1 and mSm3, a SIMPER analysis of the Dice similarity matrix was finally performed among five entities: mSm1, mSm3, and the three "intermediate" sections Palomino Ridge, Crittenden Springs and WIL 9/14. Overall average

304 dissimilarities are shown in Table 3 and confirm the intermediate and gradual
305 structure of cluster mSm2, with Palomino Ridge more closely linked to mSm3 (i.e.,
306 higher overall average dissimilarity with mSm1), WIL 9/14 showing stronger
307 affinities with mSm1 (i.e., higher overall average dissimilarity with mSm3), and
308 Crittenden Springs standing in between the two other sections (similar overall average
309 dissimilarities with southern and northern clusters).
310
311 *Distribution maps of selected taxa*. Based on the previous analyses, three main
312 clusters were statistically identified: a southern cluster (mSm3), a northern cluster
313 (mSm1), and an intermediate cluster (mSm2) including the three Nevada sections
314 Palomino Ridge, Crittenden Springs and WIL 9/14 (Figs 3, 5). Results of the
315 SIMPER analysis (Table 3 in Supplementary Data) allow the identification of the taxa
316 that most contribute to this 3-group biogeographical structure.
317 *Guodunites*, *Inyoites* and ?*Kashmirites cordilleranus* are typical examples of southern
318 taxa (Figs 6, 7), although *Inyoites* is represented in the northern cluster mSm1 by one
319 small specimen assigned to *Inyoites* sp. indet. at The Pond section (Fig. 3B).
320 Similarly, ?*Kashmirites cordilleranus* apparently occurs in one northern section
321 (Schmid Ridge). However, this report is based on five specimens with a tentative
322 assignment, only. Conversely, *Meekoceras cristatum*, *Wyomingites*, *Arctoceras*
323 *tuberculatum*, *Euflemingites*, and *Submeekoceras mushbachanum* are examples of
324 northern taxa (Figs 6, 7), even if the latter is represented also in the southern cluster
325 mSm3 by one specimen from Mineral Mountains section.
326 Nearly all the taxa characteristic of the southern part or the northern part coexist in the
327 intermediate group represented by the Nevada sections Palomino Ridge, Crittenden
328 Springs, and WIL 9/14 (Figs 6, 7). This biogeographically intermediate group also
329 contains a few endemic taxa, such as *Palominoceras nevadanum* and *Preflorianites*
330 (Figs 6, 7). The case of *Preflorianites* is a less clear-cut one than that of *P.*
331 *nevadanum* because a few specimens occur in one of the northern sections
332 (Georgetown). Other middle Smithian taxa such as the emblematic *Meekoceras*
333 *gracilitatis*, *Juvenites* and *Owenites* show a widespread distribution within the
334 western USA basin (Figs. 6, 7). However, differences in relative abundance do exist
335 (see below). Absence of these widespread taxa in a few sections possibly results from
336 still insufficient sampling effort.
337

Taxonomic diversity. The taxonomic diversity analysis achieved using the evenness index 1 – *D* (Fig. 8) based on 11 taxa within 15 sections (see above, 'Data and Methods') allows the quantitative characterization of three main groups. A first group gathers sections with high taxonomic evenness (1 – *D* values > 0.74). All southern and intermediate sections but CS 23, and only one northern section (Georgetown) pertain to this group. A second group corresponding to moderate taxonomic evenness values ranging from 0.58 to 0.74 includes most of northern sections and no southern or intermediate sections. Last, a third group comprises sections with low taxonomic evenness (1 – *D* < 0.56; Hot Springs, CS 23, Grizzly Creek and possibly also Georgetown Canyon). Notably, all sections corresponding exclusively to facies D (Table 2) fall in this group.

Relative abundance analysis. Comparisons of taxon relative abundances (including 95% Confidence Intervals on sample proportions) for each of the 11 taxa analysed (see above, 'Data and Methods') are shown in Figures 9, 10. *Dieneroceras*, ?*Kashmirites cordilleranus*, *Guodunites*, and *Inyoites* (Fig. 9) display an overall S/N decreasing gradient in relative abundance (i.e., southern sections with high proportions, Nevada sections with intermediate proportions, and northern sections with proportions close or equal to zero).

Regarding *Dieneroceras*, sections departing from this S/N decreasing gradient are CS 23 and Georgetown. Indeed, CS 23 is the only Nevada section where *Dieneroceras* is absent so far. Besides, Georgetown shows a much higher *Dieneroceras* abundance than all other northern sections.

Inyoites presents two minor outliers with respect to its clear S/N decreasing gradient. First, Crittenden Springs exhibits an especially low *Inyoites* abundance among Nevada sections. Second, *Inyoites* is absent in all northern sections, except at The Pond, although this occurrence is based on a unique specimen without species assignment.

?*Kashmirites cordilleranus* is recorded in only one northern section (Schmid Ridge), based on the identification of only five, rather poorly preserved specimens. Among the Nevada sections, CS 23 and Crittenden Springs have values closer to those of northern sections than to those of other Nevada sections.

Last, *Guodunites* occurs only in Palomino Ridge among Nevada sections. *Guodunites* is apparently absent from all northern sections. As noticed from previous analyses,

372 Palomino Ridge has close affinities with southern sections. Therefore, *Guodunites*
373 stands as a taxon with strong southern affinities, showing an abrupt S/N decreasing
374 trend in relative abundance.
375 A very weak S/N decreasing gradient can be tentatively identified for *Owenites*, with
376 low abundances in southern and Nevada sections and null abundances in northern
377 sections, with the exception of Hot Springs, Crittenden Springs, Georgetown Canyon
378 and Georgetown (Fig. 9).
379 Conversely, *Meekoceras gracilitatis*, *Submeekoceras mushbachanum* and *Juvenites*
380 (Figs. 9, 10) display a more or less robust N/S decreasing gradient in relative
381 abundances (i.e., southern sections with low to null proportions, Nevada sections with
382 intermediate proportions, and northern sections with high proportions). CS 23 is an
383 obvious outlier in the distribution of *Meekoceras gracilitatis*, showing a very low
384 abundance compared with other Nevada sections. Northern sections characterized by
385 facies D (Hot Springs, Grizzly Creek and Georgetown Canyon) have much lower *M.*
386 *gracilitatis* abundances than other northern sections. Finally, Georgetown has a
387 significantly lower abundance compared with other northern sections belonging to
388 facies C.
389 Likewise, northern sections with facies D display much lower abundances of
390 *Submeekoceras mushbachanum* than other northern sections. Interestingly,
391 Georgetown shows once again a significantly lower abundance compared with other
392 northern sections with facies C. Besides, the two southern sections show null
393 abundances in *S. mushbachanum*, and among Nevada sections, it is only known from
394 WIL 9/14. As exemplified in previous analyses, WIL 9/14 has close affinities with
395 northern sections. Therefore, *S. mushbachanum* emerges as a taxon with strong
396 northern affinities, showing an abrupt N/S decreasing trend in relative abundance.
397 *Juvenites* shows highest relative abundances in all sections with facies D (Hot
398 Springs, Grizzly Creek and Georgetown Canyon). Regardless of those sections, a
399 weak N/S decreasing trend can be identified, with only Crittenden Springs and CS 23
400 having much higher abundances compared to other Nevada and southern sections.
401 Regarding *Wyomingites*, three sections (Schmid Ridge, 2S and The Pond) show much
402 higher abundances than all other sections (Fig. 10). Noteworthy, these sections are
403 close to each others (Fig. 2) and could be treated as a single section because of the
404 lateral extension of the same fossiliferous beds. *Wyomingites* is absent in all other
405 northern sections except Grizzly Creek; it occurs only in WIL 9/14 among the Nevada

sections. *Wyomingites* can therefore be considered as a 'local' taxon restricted to the Schmid Ridge area, with a limited or patchy distribution.

Only a single section (WIL 9/14) shows a much higher abundance of *Arctoceras tuberculatum* than all other sections (Fig. 10). Otherwise, no specific pattern is emerging, except that this taxon is not recorded so far from the southern sections. Finally, no pattern can be found for *Anaflemingites*, except that this taxon is extremely rare in southern sections and that Georgetown has a relatively high abundance compared with other northern sections (Fig. 10).

Influence of facies and depositional environment on abundance data. We investigated a potential relationship between facies, depositional environments and taxonomic compositions by grouping the 15 sections analysed for abundances into the four categories of facies-based sets. A (one-way) ANOSIM test contrasting these four groups indicates significant overall abundance differences among the four clusters ($R = 0.35$, $p = 0.014$), driven by the abundance differences between the 'facies A' and 'facies C' groups, as well as between the 'facies A' and 'facies D' groups (Table 4 in Supplementary Data). Based on a SIMPER analysis (Table 5 in Supplementary Data), *Guodunites*, *Inyoites*, *Meekoceras gracilitatis*, *Dieneroceras* and *Juvenites* are identified as the main taxa contributing to the differences in abundance between the 4 facies groups.

Late Smithian

So far, few sections have yielded a statistically meaningful amount of late Smithian ammonoids, with none in the northern part of the basin. Using the available information, a two-group (one-way) ANOSIM test with one group including southern sections (Confusion Range and Black Rock Canyon) and another group gathering all other sections returned a non-significant difference in terms of faunal assemblages ($R = -0.1296$, $p = 0.74$). For relative abundances, too few sections have sufficiently large samples, thus preventing any sound statistical analysis.

DISCUSSION

Our results show that middle Smithian ammonoids of the western USA basin were geographically organized in terms of both distribution and abundance. The main pattern is the biogeographical distinction between a southern and a northern cluster. Some taxa are indeed confined to a single sub-basin (e.g., *Guodunites* and *Inyoites* in the southern part; *Wyomingites* and *Meekoceras cristatum* in the northern part; Figs 6, 7). Although some taxa are common to both sub-basins (e.g., *Juvenites*, *Owenites* and *Meekoceras gracilitatis*), only the "intermediate" sections in northeastern Nevada exhibit a mixed composition (Figs 5–7). Regarding abundance, many taxa display a geographical gradient whose maximum is either in the southern or in the northern cluster (Figs 9, 10). This N/S structuring in the distribution and abundance of middle Smithian ammonoids echoes pronounced spatial differences in depositional settings identified for the same time interval (Caravaca *et al*. in press, figs 3a, 4). From a palaeogeographical point of view, these authors postulated the existence of a W/E basement topographic high running across central-northern Utah, which may have contributed to the N/S structuring even if the southern and northern sub-basins shared modest bathymetries.

Facies and depositional environments as potential drivers of middle Smithian ammonoid assemblages

Sections with facies A: an influence of siliciclastics in the southern sub-basin?

Guodunites, *Inyoites* and *Dieneroceras*, along with ?*Kashmirites cordilleranus*, are strongly related to sections characterized by facies A (Fig. 9, Table 5 in Supplementary Data). All sections in the southern sub-basin and the Nevada Palomino Ridge section share this facies (Table 2). Nevertheless, significant differences in abundance are observed for these four taxa between the southern sections and Palomino Ridge, with constantly lower values for the latter (Fig. 9). A unique feature of facies A is the presence of siltstones (Fig. 4, Table 2), indicative of significant siliciclastic inputs mixed with the carbonate-rich fraction. It can be assumed that particular environmental parameters hardly detectable through a facies analysis (e.g., local nutrient availability, seawater temperature and salinity; for the latter, see Banham & Mountney 2013) were associated with those terrigenous inputs. We can thus hypothesize that the clastic load of the water column induced the segregation of taxa between the southern and northern parts of the basin; the abundant *Dieneroceras*,

Inyoites, ?*Kashmirites cordilleranus* and *Guodunites* in the south being presumably more tolerant with respect to this abiotic parameter. As the relative siliciclastic fraction mixed with carbonate gradually decreased northwards, the relative abundance of southern taxa gradually decreased accordingly, with intermediate values in Nevada sections (e.g., Palomino Ridge) and low to null values in northern sections. Given that *Guodunites* occurs only in sections with facies A, the abundance of this taxon probably reflects preponderant environmental parameters of the southern sub-basin.

Sections with facies C and northern seawater parameters. *Submeekoceras mushbachanum*, *Wyomingites* and especially *Meekoceras gracilitatis* are apparently strongly associated with sections belonging to facies C (Table 5 in Supplementary Data). Most sections in the northern sub-basin and the Nevada section Crittenden Springs fall within this category of facies (Table 2). As specific abiotic parameters that may have controlled the distribution of ammonoids within this facies were not identified, we suggest that the absence in ammonoid-rich northern environments of components such as siltstones locally fostered the abundance of *Meekoceras gracilitatis* and *Submeekoceras mushbachanum*. Nevertheless, significant differences in abundance are observed for these three taxa between the northern facies C sections and Crittenden Springs, with constantly lower values for the latter (Figs 9, 10). This emphasizes the intermediate position of Crittenden Springs.

Only Schmid Ridge and its closest neighbouring sections The Pond and 2S exhibit significant relative abundances for *Wyomingites* (Fig. 9). Sparse other known occurrences of *Wyomingites* are in Grizzly Creek and WIL9/14 only, suggesting that appropriate conditions for its proliferation were essentially met in Schmid Ridge, The Pond and 2S. *Juvenites* was also probably favoured in the north, but its abundance pattern is difficult to interpret due to potential taphonomic biases maybe linked to its peculiar sphaeroconic morphology (see below).

Georgetown: an exception to facies C. Georgetown often shows a distinct pattern of relative abundances compared with other northern sections with facies C (Figs 9, 10). Additionally, the high taxonomic evenness value for this section is unexpected, because it is closer to southern and most Nevada sections (Fig. 8). Noteworthy, even though Georgetown and other sections with facies C are all characterized by proximal storm-induced deposits, these occur in a deeper setting at Georgetown. We

hypothesize here that at Georgetown, the unusual evenness value, linked with the unusual proportions of *Dieneroceras*, *M. gracilitatis*, *S. mushbachanum* and *Owenites* (compared with northern sections with facies C), is due to a peculiar combination of bathymetry and storm-induced deposits.

Sections with facies B: influence of storm-induced deposits. Among the Nevada sections, CS 23 often exhibits peculiar patterns of abundance (Figs 9, 10). CS 23 and WIL9/14 belong to facies B, which corresponds to amalgamated storm-induced deposits found on palaeotopographic highs (Table 2). As CS23 and WIL9/14 do not show similar compositions, it can be assumed that the ammonoid material from each section originated from two different depositional environments, before being taphonomically altered by storms. Ammonoid material from CS 23 probably comes from a depositional environment close to that of northern sections with facies D, explaining that CS 23 clusters with northern sections in NJ and NMDS analyses, and not with close sections from Nevada (Palomino Ridge, Crittenden Springs and WIL9/14; Fig. 5).

Regarding WIL9/14, we argue that the much higher value of *Arctoceras tuberculatum* compared to all other sections cannot be only explained by a taphonomic bias (e.g., mechanical sorting by storms). A primary ecological affinity of this taxon for the corresponding depositional environment likely accounts for its spectacular proportion in WIL9/14.

High energy depositional setting: facies D and the peculiar case of sphaerocones. Facies D corresponds to a high hydrodynamic environment (Table 2), where taphonomic biases linked to shell morphology could be predominant. We hypothesize that large, compressed shells such as *Meekoceras gracilitatis* and *Submeekoceras mushbachanum*, as well as serpenticonic shells such as *Dieneroceras* and ?*K. cordilleranus* were selectively broken in this high energy depositional setting, resulting in a reduced number of complete, identifiable specimens. This possibly explains the lack of *Dieneroceras* and ?*K. cordilleranus* in CS 23 (as opposed to intermediate abundances in most Nevada sections; Fig. 9), whose depositional environment is assumed to be close to that of sections with facies D (see above). It would also elucidate the lower proportions of *M. gracilitatis* in CS 23 and in northern

sections with facies D compared to other northern sections, although the extremely low proportion of *M. gracilitatis* in Hot Springs remains unexplained.

Conversely, small, globose and mechanically more resistant shells (e.g., *Juvenites*) better resisted the high-energy hydrodynamic conditions of facies D. The SIMPER analysis shows that *Juvenites* is preferentially bounded with facies D (Table 5 in Supplementary Data). Specimens of other taxa also having a somewhat globose shell shape (e.g., *Owenites*), are present in the same depositional environment but are often broken. There is neither taphonomic nor sedimentological evidence for lateral transport of shells in facies D, which suggests that *Juvenites* was proliferating in this high-energy, very shallow habitat, regardless of any taphonomic bias that may have increased its relative abundance.

Sphaerocones (including globose forms like *Juvenites*) were interpreted either as (i) inhabitants of low-energy offshore environments (Jacobs 1992; Jacobs *et al*. 1994), (ii) vertical migrants (Westermann 1996), or (ii) slow demersal swimmers (Swan & Saunders 1987). Their high abundance in Facies D stands in striking contrast with all these assumptions where smooth sphaerocones are assumed to be less adapted to shallow, high-energy settings. Assigning a functional explanation to a given shell morphology (compare, e.g., Brayard & Escarguel 2013 and Zacaï *et al*. 2016 for similar analyses leading to divergent conclusions) remains extremely speculative for nektonic organisms. Wang & Westermann (1993) also stated that "the synecological record indicates that the sphaerocones often lived in low-diversity or monospecific communities". However, in our case study, the low diversity (*sensu* evenness) observed in sections where *Juvenites* is predominant (CS 23 and sections with facies D; Fig. 8) results from the mechanical sorting that is frequent in these high-energy subtidal shoals.

All other analysed taxa support the non-existence of relationship between *ad hoc* morpho-functional categories and facies in our dataset. The sphaerocone *Paranannites* is too sparse for a robust assessment. Although the shell morphology of *Owenites* is somewhat akin to that of *Juvenites*, a high abundance of *Owenites* is only observed in Hot Springs among sections with facies D. This peculiar abundance cannot be explained by any consistent relation between shell shape and depositional environment across different taxa. Similarly, the unusually high proportion of *Owenites* in Crittenden Springs (facies C) is at variance with such a simplistic relation.

574

575 *Late Smithian*

576

577 Available data do not indicate any significant structuring within the western USA
578 basin for late Smithian faunal assemblages. Noteworthy, the late Smithian open-
579 marine bioclastic limestones and shales of the Thaynes Group regionally mark the
580 Early Triassic maximum flooding (Collinson & Hasenmueller 1978; Carr & Paull
581 1983; Paull & Paull 1993; Lucas *et al*. 2007; Vennin *et al*. 2015; Olivier et al. 2014,
582 2016), characterized by the presence of the iconic ammonoid genus *Anasibirites* and
583 other typical late Smithian ammonoids (Lucas *et al*. 2007; Brayard *et al*. 2013; Jattiot
584 *et al*. 2016, 2017). This large distribution within the entire western USA basin is
585 independent from depositional environments. At a global scale, the late Smithian
586 ammonoid extinction was accompanied by remarkable cosmopolitan distributions,
587 irrespective of the local peculiarities of depositional settings (e.g., *Hemiprionites*,
588 *Wasatchites, Xenoceltites* and *Anasibirites*; Tozer 1982; Brayard et al. 2006; Jattiot *et*
589 *al*. 2016). Therefore, the absence of ecological partitioning in the late Smithian of the
590 western USA basin reflects the overriding imprint (diversity collapse and
591 cosmopolitan distributions) of this global extinction.

592

593 **CONCLUSION**

594

595 Our work has shown that the differentiation recognized between the northern part and
596 the southern part of the western USA basin based on sedimentary evolution and
597 subsidence rates (Caravaca *et al*. in press), is also captured by the ecological
598 structuration of middle Smithian ammonoid faunas. Occurrences of some species are
599 limited to the southern part of the basin, whereas occurrences of other species are
600 restricted to the northern part of the basin. N/S or S/N gradients of relative abundance
601 are observed for some taxa. In some cases, a concordance between characteristics of
602 depositional environments (e.g., clastic load of the water column and energy level)
603 and the relative abundance of some taxa is clearly emerging. Conversely, the absence
604 of ecological partitioning in the late Smithian does not relate to the nature of
605 depositional settings but reflects the overriding consequences of the global late
606 Smithian ammonoid extinction and associated cosmopolitan distributions. As far as

Early Triassic ammonoids are concerned, our quantitative analyses also question the traditional *ad hoc* morpho-functional interpretations of the shell shape.

Acknowledgements. The final version of this paper benefited from constructive reviews by Alistair McGowan, Sally Thomas and an anonymous referee. Support from the Swiss NSF (project 160055 to HB), from the Claraz Fund (to HB) and from the French ANR-13-JS06-0001-01 AFTER project (to AB) is deeply acknowledged.

DATA ARCHIVING STATEMENT

The following supplementary data files are available in the Dryad Digital Repository:

REFERENCES

BANHAM, S. G. and MOUNTNEY, N. P. 2013. Controls on fluvial sedimentary architecture and sediment-fill state in salt-walled mini-basins: Triassic Moenkopi Formation, Salt Anticline Region, SE Utah, USA. *Basin Research*, **25**, 709–737.

BARESEL, B., BUCHER, H., BROSSE, M., CORDEY, F., GUODUN, K. and SCHALTEGGER, U. 2017. Precise age for the Permian–Triassic boundary in South China from high-precision U-Pb geochronology and Bayesian age–depth modeling. *Solid Earth*, **8**, 361–378.

BASELGA, A. 2010. Partitioning the turnover and nestedness components of beta diversity. *Global Ecology and Biogeography*, **19**, 134–143.

— 2012. The relationship between species replacement, dissimilarity derived from nestedness, and nestedness. *Global Ecology and Biogeography*, **21**, 1223–1232.

BATT, R. J. 1989. Ammonite shell morphotype distributions in the Western Interior Greenhorn Sea and some paleoecological implications. *Palaios*, **4**, 32–42.

— 1993. Ammonite morphotypes as indicators of oxygenation in a Cretaceous epicontinental sea. *Lethaia*, **26**, 49–63.

BAYER, U. and MCGHEE, G. R. J. 1984. Iterative evolution of Middle Jurassic ammonite faunas. *Lethaia*, **17**, 1–16.

BRAYARD, A. and BUCHER, H. 2008. Smithian (Early Triassic) ammonoid faunas from northwestern Guangxi (South China): taxonomy and biochronology. *Fossils and Strata*, **55**, 1–179.

— — 2015. Permian-Triassic extinctions and rediversifications. 465–473. *In* KLUG, C., KORN, D., DE BAETS, K., KRUTA, I. and MAPES, R. H. (eds). *Ammonoid Paleobiology: From macroevolution to paleogeography*. Topics in Geobiology, **44**, Springer, Dordrecht, 599 pp.

— and ESCARGUEL, G. 2013. Untangling phylogenetic, geometric and ornamental imprints on Early Triassic ammonoid biogeography: a similarity-distance decay study. *Lethaia*, **46**, 19–33.

— BUCHER, H., ESCARGUEL, G., FLUTEAU, F., BOURQUIN, S. and GALFETTI, T. 2006. The Early Triassic ammonoid recovery: paleoclimatic significance of diversity gradients. *Palaeogeography, Palaeoclimatology, Palaeoecology*, **239**, 374–395.

— ESCARGUEL, G. and BUCHER, H. 2007. The biogeography of Early Triassic ammonoid faunas: clusters, gradients, and networks. *Geobios*, **40**, 749–765.

— — — MONNET, C., BRÜHWILER, T., GOUDEMAND, N., GALFETTI, T. and GUEX, J. 2009*a*. Good genes and good luck: ammonoid diversity and the end-Permian mass extinction. *Science*, **325**, 1118–1121.

— BRÜHWILER, T., BUCHER, H. and JENKS, J. 2009*b*. *Guodunites*, a low-palaeolatitude and trans-Panthalassic Smithian (Early Triassic) ammonoid genus. *Palaeontology*, **52**, 471–481.

— ESCARGUEL, G., BUCHER, H. and BRÜHWILER, T. 2009*c*. Smithian and Spathian (Early Triassic) ammonoid assemblages from terranes: paleoceanographic and paleogeographic implications. *Journal of Asian Earth Sciences*, **36**, 420–433.

— BYLUND, K. G., JENKS, J. F., STEPHEN, D. A., OLIVIER, N., ESCARGUEL, G., FARA, E. and VENNIN, E. 2013. Smithian ammonoid faunas from Utah: implications for Early Triassic biostratigraphy, correlation and basinal paleogeography. *Swiss Journal of Palaeontology*, **132**, 141–219.

— ESCARGUEL, G., MONNET, C., JENKS, J. F. and BUCHER, B. 2015. Biogeography of Triassic ammonoids. 163–187. *In* KLUG, C., KORN, D., DE BAETS, K., KRUTA, I. and MAPES, R. H. (eds). *Ammonoid Paleobiology: From macroevolution to paleogeography*. Topics in Geobiology, **44**, Springer, Dordrecht, 599 pp.

BROSSE, M., BRAYARD, A., FARA, E. and NEIGE, P. 2013. Ammonoid recovery after the Permian-Triassic mass extinction: a re-exploration of morphological and phylogenetic diversity patterns. *Journal of the Geological Society*, **170**, 225–236.

BRÜHWILER, T., BUCHER, H., BRAYARD, A. and GOUDEMAND, N. 2010*a*. High-resolution biochronology and diversity dynamics of the Early Triassic ammonoid recovery: the Smithian faunas of the Northern Indian Margin. *Palaeogeography, Palaeoclimatology, Palaeoecology*, **297**, 491–501.

— — and GOUDEMAND, N. 2010*b*. Smithian (Early Triassic) ammonoids from Tulong, South Tibet. *Geobios*, **43**, 403–431.

— — — and GALFETTI, T. 2012*a*. Smithian (Early Triassic) ammonoids faunas from Exotic Blocks from Oman: taxonomy and biochronology. *Palaeontographica Abteilung A*, **296**, 3–107.

— — WARE, D., HERMANN, E., HOCHULI, P. A., ROOHI, G., REHMAN, K. and YASEEN, A. 2012*b*. Smithian (Early Triassic) ammonoids from the Salt Range. *Special Papers in Palaeontology*, **88**, 1–114.

— — and KRYSTYN, L. 2012*c*. Middle and late Smithian (Early Triassic) ammonoids from Spiti, India. *Special Papers in Palaeontology*, **88**, 115–174.

BULOT, L. G. 1993. Stratigraphical implications of the relationships between ammonites and facies: examples taken from the Lower Cretaceous (Valanginian – Hauterivian) of the western Tethys. *In* HOUSE, M. R. (ed.). *The Ammonoidea: environment, ecology, and evolutionary change*. Systematics Association Special Volume, Clarendon Press, Oxford, 354 pp.

CARAVACA, G., BRAYARD, A., VENNIN, E., GUIRAUD, M., LE POURHIET, L., GROSJEAN, A. S., THOMAZO, C., OLIVIER, N., FARA, E., ESCARGUEL, G., JENKS, J. F., BYLUND, K. G. and STEPHEN, D. A. (in press). Controlling factors for differential subsidence in the Sonoma Foreland Basin (Early Triassic, western USA). *Geological Magazine*, 1–25.

CARR, T. C. and PAULL, R. K. 1983. Early Triassic stratigraphy and paleogeography of the Cordilleran miogeocline. *Rocky Mountain Symposium*, **2**, 39–55.

CLARKE, K. R. 1993. Non-parametric multivariate analyses of changes in community structure. *Australian Journal of Ecology*, **18**, 117–143.

COLLINSON, J. W. and HASENMUELLER, W. A. 1978. Early Triassic paleogeography and biostratigraphy of the Cordilleran miogeosyncline. *Pacific Coast Paleogeography Symposium*, **2**, 175–187.

— KENDALL, C. and MARCANTEL, J. B. 1976. Permian-Triassic boundary in eastern Nevada and west-central Utah. *Geological Society of America Bulletin*, **87**, 821–824.

COMPANY, M. 1987. Los ammonites del valanginiense del sector oriental de las cordilleras béticas (SE de España). PhD thesis, University of Granada, Granada, 344 pp.

DAGYS, A. 1988. Major features of the geographic differentiation of Triassic ammonoids. 341–349. *In* WIEDMANN, J. and KULLMANN, J. (eds). *Cephalopods–present and past*. Schweizerbart'sche Verlagsbuchhandlung, Stuttgart.

FIELD, J. G., CLARKE, K. R. and WARWICK, R. M. 1982. A practical strategy for analysing multispecies distribution patterns. *Marine Ecology Progress Series*, **8**, 37–52.

GALFETTI, T., BUCHER, H., OVTCHAROVA, M., SCHALTEGGER, U., BRAYARD, A., BRÜHWILER, T., GOUDEMAND, N., WEISSERT, H., HOCHULI, P. A., CORDEY, F. and GUODUN, K. 2007. Timing of the Early Triassic carbon cycle perturbations inferred from new U–Pb ages and ammonoid biochronozones. *Earth and Planetary Science Letters*, **258**, 593–604.

GILLULY, J. and REESIDE, J. B. 1927. Sedimentary rocks of the San Rafael Swell and some adjacent areas in eastern Utah. *U.S. Geological Survey Professional Paper*, **150-D**, 61–110.

HALLAM, A. 1996. Major bio-events in the Triassic and Jurassic. 265–283. *In* WALLISER, O. H. (ed.). *Global Events and Event Stratigraphy in the Phanerozoic: Results of the International Interdisciplinary Cooperation in the IGCP-Project 216 "Global Biological Events in Earth History"*. Springer-Verlag, Berlin, 333 pp.

HAMMER, Ø., HARPER, D. and PAUL, D. 2001. Past: paleontological statistics software package for education and data analysis. *Palaeontologia Electronica*. Available from: http://folk.uio.no/ohammer/past/.

HERMANN, E., HOCHULI, P. A., BUCHER, H., BRÜHWILER, T., HAUTMANN, M., WARE, D. and ROOHI, G. 2011. Terrestrial ecosystems on North Gondwana in the aftermath of the end-Permian mass extinction. *Gondwana Research*, **20**, 630–637.

HURLBERT, S. H. 1971. The nonconcept of species diversity: a critique and alternative parameters. *Ecology*, **52**, 577–586.

JACOBS, D. K. 1992. Shape, drag, and power in ammonoid swimming. *Paleobiology*, **18**, 203–220.

— LANDMAN, N. H. Y. and CHAMBERLAIN, J. A. 1994. Ammonite shell shape covaries with facies and hydrodynamics: iterative evolution as a response to changes in basinal environment. *Geology*, **22**, 905–908.

JATTIOT, R., BUCHER, H., BRAYARD, A., MONNET, C., JENKS, J. F. and HAUTMANN, M. 2016. Revision of the genus *Anasibirites* Mojsisovics (Ammonoidea): an iconic and cosmopolitan taxon of the late Smithian (Early Triassic) extinction. *Papers in Palaeontology*, **2**, 155–188.

— BUCHER, H., BRAYARD, A., BROSSE, M., JENKS, J. F. and BYLUND, K. G. 2017. Smithian ammonoid faunas from northeastern Nevada: implications for Early Triassic biostratigraphy and correlation within the western USA basin. *Palaeontographica Abteilung A*, **309**, 1–89.

JENKS, J. F., BRAYARD, A., BRÜHWILER, T. and BUCHER, H. 2010. New Smithian (Early Triassic) ammonoids from Crittenden Springs, Elko County, Nevada: Implications for taxonomy, biostratigraphy and biogeography. *New Mexico Museum of Natural History and Science Bulletin*, **48**, 1–41.

KAWABE, F. 2003. Relationship between mid-Cretaceous (upper Albian-Cenomanian) ammonoid facies and lithofacies in the Yezo forearc basin, Hokkaido, Japan. *Cretaceous Research*, **24**, 751–763.

KOLEFF, P., GASTON, K. J. and LENNON, J. J. 2003. Measuring beta diversity for presence–absence data. *Journal of Animal Ecology*, **72**, 367–382.

KLUG, C. 2002. Conch parameters and habitats of Emsian and Eifelian ammonoids from the Tafilalt (Morocco) and their relation to global events. *Abhandlungen der Geologischen Bundesantalt*, **57**, 523–538.

— and KORN, D. 2004. The origin of ammonoid locomotion. *Acta Palaeontologica Polonica*, **49**, 235–242.

KRUSKAL, J. B. 1956. On the shortest spanning subtree of a graph and the traveling Salesman problem. *Proceedings of the American Mathematical Society*, **7**, 48–50.

LEGENDRE, P. and LEGENDRE, L. 2012. *Numerical ecology*, 3rd edn. Developments in Environmental Modeling, **24**, Elsevier, Amsterdam, 1006 pp.

LUCAS, S. G., KRAINER, K. and MILNER, A. R. 2007. The type section and age of the Timpoweap Member and stratigraphic nomenclature of the Triassic Moenkopi Group in Southwestern Utah. *New Mexico Museum of Natural History and Science Bulletin*, **40**, 109–117.

MANSFIELD, G. R. and GIRTY, G. H. 1927. Geography, geology, and mineral resources of part of southeastern Idaho. *U.S. Geological Survey Professional Paper*, **152**, 1–447.

MCKEE, E. D. 1954. Stratigraphy and history of the Moenkopi Formation of Triassic age. *Geological Society of America Memoirs*, **61**, 1–126.

MONNET, C., DE BAETS, K. and KLUG, C. 2011. Parallel evolution controlled by adaptation and covariation in ammonoid cephalopods. *BMC evolutionary Biology*, **11**, 115.

NEIGE, P., MARCHAND, D. and BONNOT, A. 1997. Ammonoid morphological signal versus sea-level changes. *Geological Magazine*, **134**, 261–264.

OLIVIER, N., BRAYARD, A., FARA, E., BYLUND, K. G., JENKS, J. F., VENNIN, E., STEPHEN, D. A. and ESCARGUEL, G. 2014. Smithian shoreline migrations and depositional settings in Timpoweap Canyon (Early Triassic, Utah, USA). *Geological Magazine*, **151**, 938–955.

— — VENNIN, E., ESCARGUEL, G., FARA, E., BYLUND, K. G., JENKS, J. F., CARAVACA, G., STEPHEN, D. A. 2016. Evolution of depositional settings in the Torrey area during the Smithian (Early Triassic, Utah, USA) and their significance for the biotic recovery. *Geological Journal*, **51**, 600–626.

OVTCHAROVA, M., BUCHER, H., SCHALTEGGER, U., GALFETTI, T., BRAYARD, A. and GUEX, J. 2006. New Early to Middle Triassic U–Pb ages from South China: calibration with ammonoid biochronozones and implications for the timing of the Triassic biotic recovery. *Earth and Planetary Science Letters*, **243**, 463–475.

— GOUDEMAND, N., HAMMER, Ø., GUODUN, K., CORDEY, F., GALFETTI, T., SCHALTEGGER, U. and BUCHER, H. 2015. Developing a strategy for accurate definition of a geological boundary through radio-isotopic and biochronological dating: the Early-Middle Triassic boundary (South China). *Earth-Science Reviews*, **146**, 65–76.

PAULL, R. A. and PAULL, R. K. 1993. Interpretation of Early Triassic nonmarine–marine relations, Utah, USA. *New Mexico Museum of Natural History and Science Bulletin*, **3**, 403–409.

PAYNE, J. L., LEHRMANN, D. J., WEI, J., ORCHARD, M. J., SCHRAG, D. P. and KNOLL, A. H. 2004. Large perturbations of the carbon cycle during recovery from the end-Permian extinction. *Science*, **305**, 506–509.

PRIM, R. C. 1957. Shortest connection networks and some generalizations. *Bell System Technical Journal*, **36**, 1389–1401.

RAUP, D. M. and CHAMBERLAIN, J. A. 1967. Equations for volume and center of gravity in ammonoid shells. *Journal of Paleontology*, **41**, 566–574.

ROMANO, C., GOUDEMAND, N., VENNEMANN, T. W., WARE, D., SCHNEEBELI-HERMANN, E., HOCHULII, P. A., BRÜHWILER, T., BRINKMANN, W. and BUCHER, H. 2013. Climatic and biotic upheavals following the end-Permian mass extinction. *Nature Geoscience*, **6**, 57–60.

SAUNDERS, W. B. and SWAN, A. R. H. 1984. Morphology and morphologic diversity of Mid-Carboniferous (Namurian) ammonoids in time and space. *Paleobiology*, **10**, 195–228.

SHIGETA, Y. and KUMAGAE, T. 2015. *Churkites*, a trans-Panthalassic Early Triassic ammonoid genus from South Primorye, Russian Far East. *Paleontological Research*, **19**, 219–236.

— and NGUYEN, H. D. 2014. Systematic paleontology: cephalopods. 65–167. *In* SHIGETA, Y., KOMATSU, T., MAEKAWA, T. and DANG, H. T. (eds). *Olenekian (Early Triassic) stratigraphy and fossil assemblages in northeastern Vietnam*. National Museum of Nature and Science Monographs, **45**, Tokyo.

— and ZAKHAROV, Y. D. 2009. Systematic paleontology: cephalopods. 44–140. *In* SHIGETA, Y., ZAKHAROV, Y., MAEDA, H. and POPOV, A. M. (eds). *The Lower Triassic system in the Abrek Bay area, South Primorye, Russia*. National Museum of Nature and Science Monographs, **38**, Tokyo.

— MAEDA, H. and ZAKHAROV, Y. D. 2009. Biostratigraphy: ammonoid succession. 24–27. *In* SHIGETA, Y., ZAKHAROV, Y., MAEDA, H. and POPOV, A. M. (eds). *The Lower Triassic system in the Abrek Bay area, South Primorye, Russia*. National Museum of Nature and Science Monographs, **38**, Tokyo.

SIMPSON, E. H. 1949. Measurement of diversity. *Nature*, **163**, 688.

905 SNEATH, P. H. A. and SOKAL, R. R. 1973. *Numerical taxonomy - the principles*
906 *and practice of numerical classification*. W.H. Freeman & Co. Ltd., San Francisco,
907 588 pp.
908
909 SOKAL, R. R. and ROHLF, F. J. 1995. *Biometry: the principles and practice of*
910 *statistics in biological research*, 3rd edn. W. H. Freeman and Co. Ltd., 896 pp.
911
912 STEPHEN, D. A., BYLUND, K. G., BYBEE, P. J. and REAM, W. J. 2010.
913 Ammonoid beds in the Lower Triassic Thaynes Formation of western Utah, USA.
914 243–252. *In* TANABE, K., SHIGETA, Y., SASAKI, T. and HIRANO, H. (eds).
915 *Cephalopods–present and past*, Tokyo.
916
917 SWAN, A. R. H. and SAUNDERS, W. B. 1987. Function and shape in late Paleozoic
918 (mid-Carboniferous) ammonoids. *Paleobiology*, **13**, 297–311.
919
920 TOZER, E. T. 1982. Marine Triassic faunas of North America: their significance for
921 assessing plate and terrane movements. *Geologische Rundschau*, **71**, 1077–1104.
922
923 VENNIN, E., OLIVIER, N., BRAYARD, A., BOUR, I., THOMAZO, C.,
924 ESCARGUEL, G., FARA, E., BYLUND, K. G., JENKS, J. F., STEPHEN, D. A. and
925 HOFMANN, R. 2015. Microbial deposits in the aftermath of the end-Permian mass
926 extinction: A diverging case from the Mineral Mountains (Utah, USA).
927 *Sedimentology*, **62**, 753–792.
928
929 WANG, Y. and WESTERMANN, G. E. G. 1993. Paleoecology of Triassic
930 ammonoids. *Geobios*, **26**, 373–392.
931
932 WANI, R. 2003. Taphofacies models for Upper Cretaceous ammonoids from the
933 Kotanbetsu area, northwestern Hokkaido, Japan. *Palaeogeography,*
934 *Palaeoclimatology, Palaeoecology*, **199**, 71–82.
935
936 WARE, D., BUCHER, H., BRAYARD, A., SCHNEEBELI-HERMANN, E. and
937 BRÜHWILER, T. 2015. High-resolution biochronology and diversity dynamics of the

Early Triassic ammonoid recovery: the Dienerian faunas of the Northern Indian Margin. *Palaeogeography, Palaeoclimatology, Palaeoecology*, **440**, 363–373.

WESTERMANN, G. E. G. 1996. Ammonoid life and habitat. 607–707. *In* LANDMAN, N. H. Y., TANABE, K. and DAVID, R. A. (eds). *Ammonoid Paleobiology*. Topics in Geobiology, **13**, Springer-Verlag US, 857 pp.

ZACAI, A., BRAYARD, A., DOMMERGUES, J. L., MEISTER, C, ESCARGUEL, G, LAFFONT, R, VRIELYNCK, B and FARA, E. 2016. Gauging scale effects and biogeographical signals in similarity distance decay analyses: an early Jurassic ammonite case study. *Palaeontology*, **59**, 671–687.

ZAKHAROV, Y. D. and ABNAVI, N. M. 2013. The ammonoid recovery after the end-Permian mass extinction: evidence from the Iran-Transcaucasia area, Siberia, Primorye, and Kazakhstan. *Acta Palaeontologica Polonica*, **58**, 127–147.

— and POPOV, A. M. 2014. Recovery of brachiopod and ammonoid faunas following the end-Permian crisis: additional evidence from the Lower Triassic of the Russian Far East and Kazakhstan. *Journal of Earth Science*, **25**, 1–44.

— SHIGETA, Y., POPOV, A. M., BURYI, G. I., OLEINIKOV, A.V., DORUKHOVSKAYA, E. A. and MIKHALIK, T. M. 2002. Triassic ammonoid succession in South Primorye: 1. Lower Olenekian *Hedenstroemia bosphorensis* and *Anasibirites nevolini* Zones. *Albertiana*, **27**, 42–64.

— BONDARENKO, L. G., SMYSHLYAEVA, O. P. and POPOV, A. M. 2013. Late Smithian (Early Triassic) ammonoids from the *Anasibirites nevolini* Zone of South Primorye, Russian Far East. *New Mexico Museum of Natural History and Science Bulletin*, **61**, 597–612.

Figure captions

FIG. 1. Chronostratigraphic subdivisions of the Early Triassic calibrated with published radiometric ages (Ovtcharova *et al*. 2006, 2015; Galfetti *et al*. 2007;

Baresel *et al*. 2017). $\delta^{13}C_{carb}$ curves and anoxic/euxinic events from Galfetti *et al*. 2007. A: *Anasibirites*, X: *Xenoceltites*, ea.: early, mi.: middle, l.: late. Simplified ammonoid diversity curve is inferred from data from Brayard *et al*. (2006, 2009*a*), Brühwiler *et al*. (2010*a*) and Ware *et al*. (2015).

FIG. 2. Early Triassic location of the western USA basin (black star). White stars indicate some other basins from which Smithian ammonoids have been documented.

FIG. 3. Palaeopositions of sampled Smithian sections within the western USA basin. A, whole western USA basin. B, inset of most northern sections. Abbreviations: HC: Hawley Creek, GC: Grizzly Creek, GR: Grays Range, RM: Reservoir Mountain, M: Monsanto, SR: Schmid Ridge, WR: Webster Range, SC: Sage Creek, GCa: Georgetown Canyon, CR: Confusion Range, PR: Pahvant Range, SRa: Star Range, GT: Georgetown, HS: Hot Springs, CS: Crittenden Springs, LWC: Lower Weber Canyon, CG: Cephalopod Gulch, FD: Fort Douglas, C: Cottonwood, PRi: Palomino Ridge, CC: Cedar City Area, BRC: Black Rock Canyon, RC: Rock Canyon, CCa: Cuts Canyon, MM: Mineral Mountains, TO: Torrey Area, SRS: San Rafael Swell, KAN: Kanarraville, WIL: Willow Creek.

FIG. 4. Thin sections of the main ammonoid-rich facies. A, ammonoid (Am)-rich floatstone in a micritic matrix associated with very fine siltstones (Palomino Ridge section). B, ammonoid-rich (Am) floatstone alternating with a bivalve-rich floatstone (WIL 9/14 section). C, ammonoid (Am) and bivalve bioaccumulation (The Pond section). D, stacked bioclastic and ammonoid (Am) packstone (Stewart Canyon section). Scale bars: 0.5 mm.

TABLE 1. Contingency table for the 11 taxa selected for the abundance-based analyses. For each taxon, the χ^2 test contrasts the raw abundance of this taxon against the raw abundance of the 10 other taxa within the 15 selected middle Smithian sections.

TABLE 2. Main facies and their corresponding depositional environments identified in the 15 middle Smithian sections selected for the analyses based on abundance data.

FIG. 5. A, Neighbour Joining tree; B, most common NMDS map obtained (378 out of 500 analysis iterations, i.e., 75%) and superimposed minimum spanning tree, with a Kruskal-stress value of 0.18. Dashed lines indicate non-significant variations in the NMDS map.

TABLE 3. Overall average dissimilarities of WIL 9/14, Palomino Ridge and Crittenden Springs with mSm1 and mSm3 clusters.

FIG. 6. Distribution maps of *Meekoceras gracilitatis*, *Meekoceras cristatum*, *Guodunites*, *Euflemingites*, *Inyoites* and *Owenites* within the western USA basin, based on palaeopositions of sampled Smithian sections.

FIG. 7. Distribution maps of *Palominoceras nevadanum*, *Wyomingites*, *Arctoceras tuberculatum*, *Juvenites*, ?*Kashmirites cordilleranus* and *Submeekoceras mushbachanum* within the western USA basin, based on palaeopositions of sampled Smithian sections.

FIG. 8. Diversity (*sensu* evenness) of the 15 analysed sections using 11 selected taxa. Square, circle, triangle, star: facies A, B, C, D sections, respectively.

FIG. 9. Relative abundances (average and 95% confidence intervals) on empirical proportions of *Dienerоceras*, *Inyoites*, ?*Kashmirites cordilleranus*, *Guodunites*, *Owenites* and *Meekoceras gracilitatis* among the 15 analysed sections. Square, circle, triangle, star: facies A, B, C, D sections, respectively.

FIG. 10. Relative abundances (average and 95% confidence intervals) on empirical proportions of *Submeekoceras mushbachanum*, *Juvenites*, *Wyomingites*, *Arctoceras tuberculatum* and *Anaflemingites* among the 15 analysed sections. Square, circle, triangle, star: facies A, B, C, D sections, respectively.

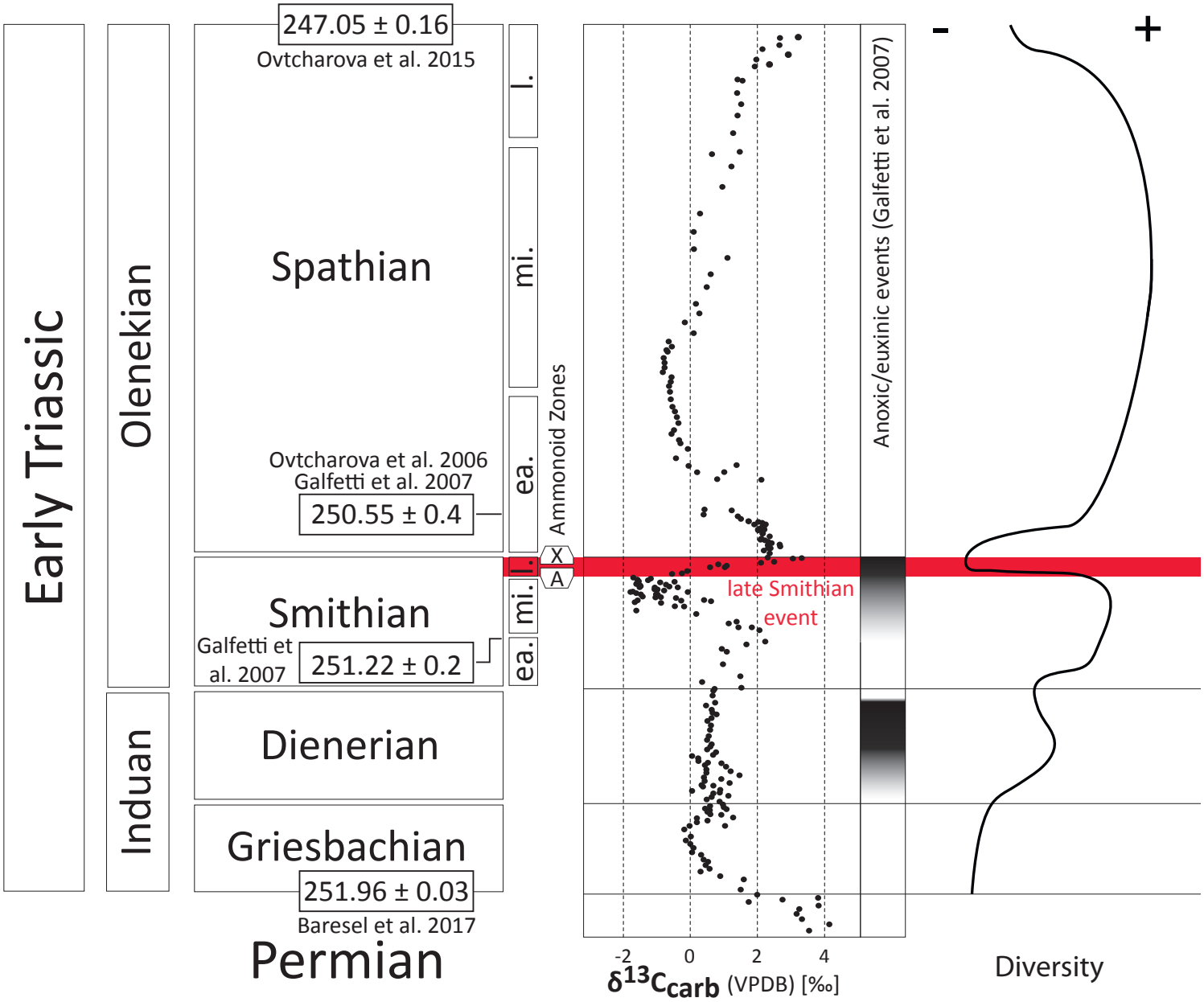
Early Triassic
Olenekian
Induan
Permian
247.05 ± 0.16
Ovtcharova et al. 2015
Spathian
Ovtcharova et al. 2006
Galfetti et al. 2007
250.55 ± 0.4
Smithian
Galfetti et al. 2007
251.22 ± 0.2
Dienerian
Griesbachian
251.96 ± 0.03
Baresel et al. 2017
l.
mi.
ea.
l.
mi.
ea.
Ammonoid Zones
X
A
late Smithian event
Anoxic/euxinic events (Galfetti et al. 2007)
-
+
-2
0
2
4
δ13Ccarb (VPDB) [‰]
Diversity

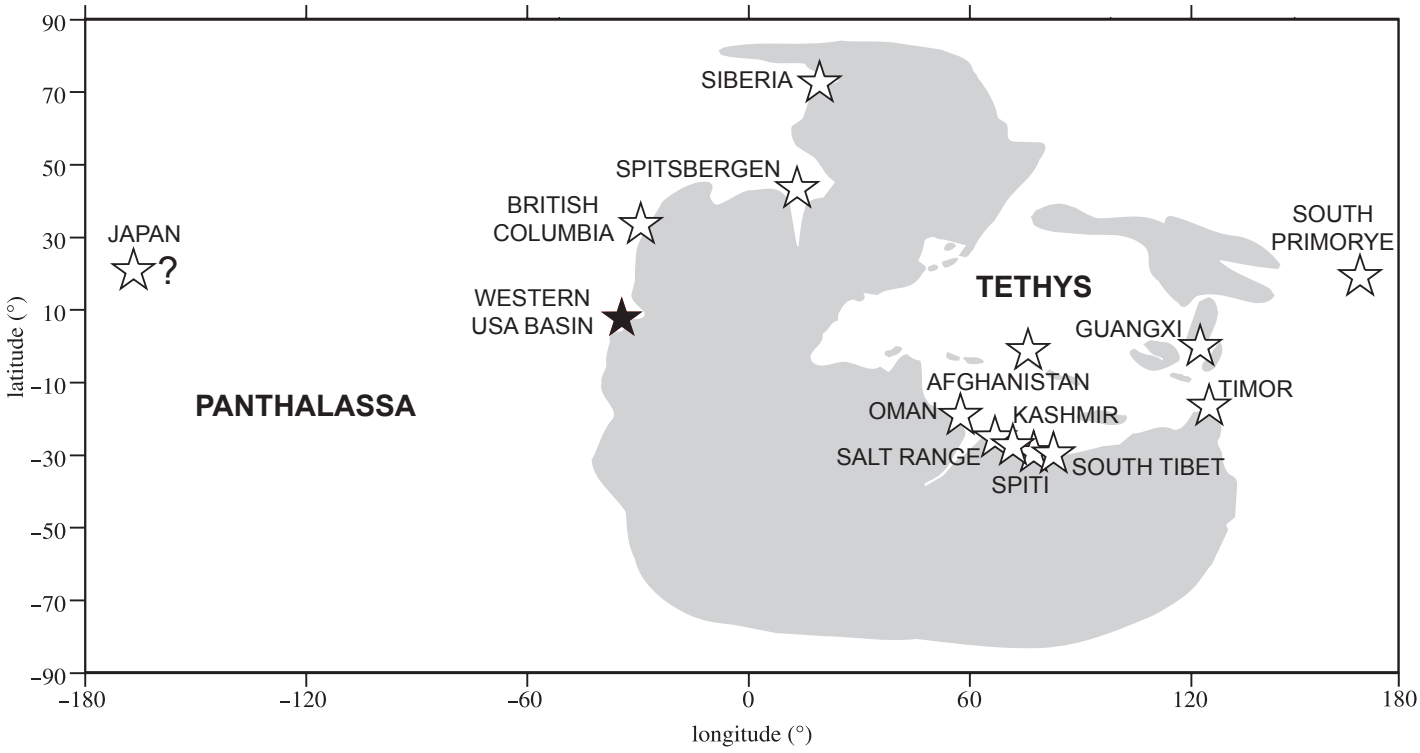
SIBERIA
SPITSBERGEN
BRITISH COLUMBIA
JAPAN
?
WESTERN USA BASIN
PANTHALASSA
TETHYS
SOUTH PRIMORYE
GUANGXI
AFGHANISTAN
TIMOR
OMAN
KASHMIR
SALT RANGE
SPITI
SOUTH TIBET
90
70
50
30
10
−10
−30
−50
−70
−90
−180
−120
−60
0
60
120
180
latitude (°)
longitude (°)

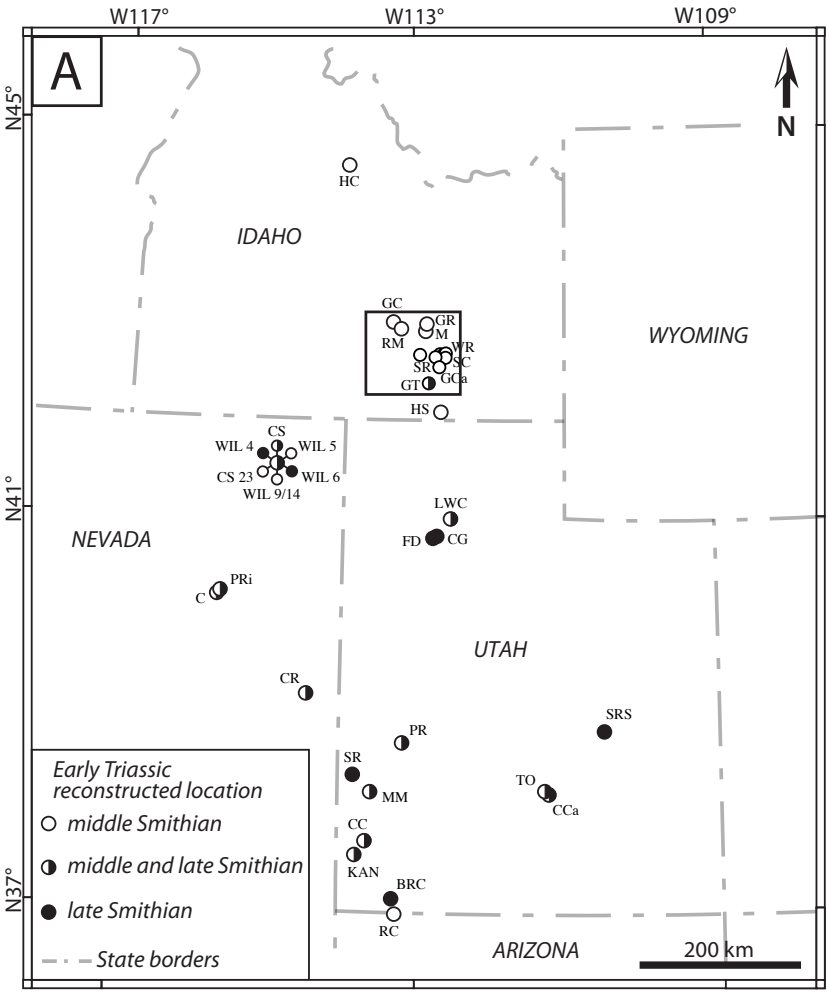
A
W117°
W113°
W109°
N45°
N41°
N37°
N
IDAHO
WYOMING
NEVADA
UTAH
ARIZONA
HC
GC
GR
M
RM
WR
SC
SR
GCa
GT
HS
CS
WIL 4
WIL 5
CS 23
WIL 6
WIL 9/14
LWC
FD
CG
PRi
C
CR
PR
SRS
SR
MM
TO
CCa
CC
KAN
BRC
RC
Early Triassic reconstructed location
middle Smithian
middle and late Smithian
late Smithian
State borders
200 km

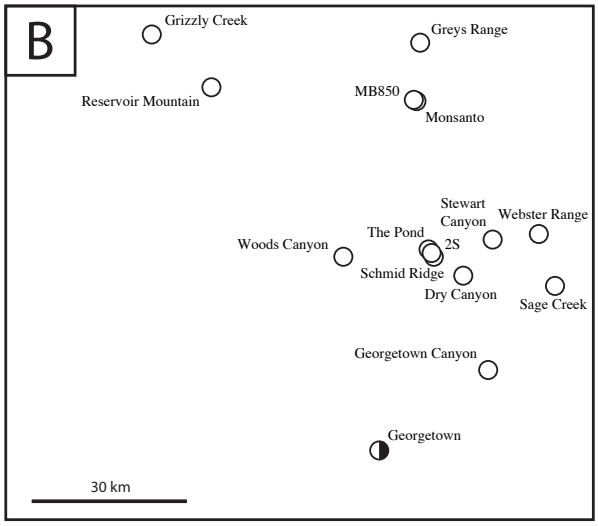
B
Grizzly Creek
Greys Range
Reservoir Mountain
MB850
Monsanto
Stewart Canyon
Webster Range
Woods Canyon
The Pond
2S
Schmid Ridge
Dry Canyon
Sage Creek
Georgetown Canyon
Georgetown
30 km

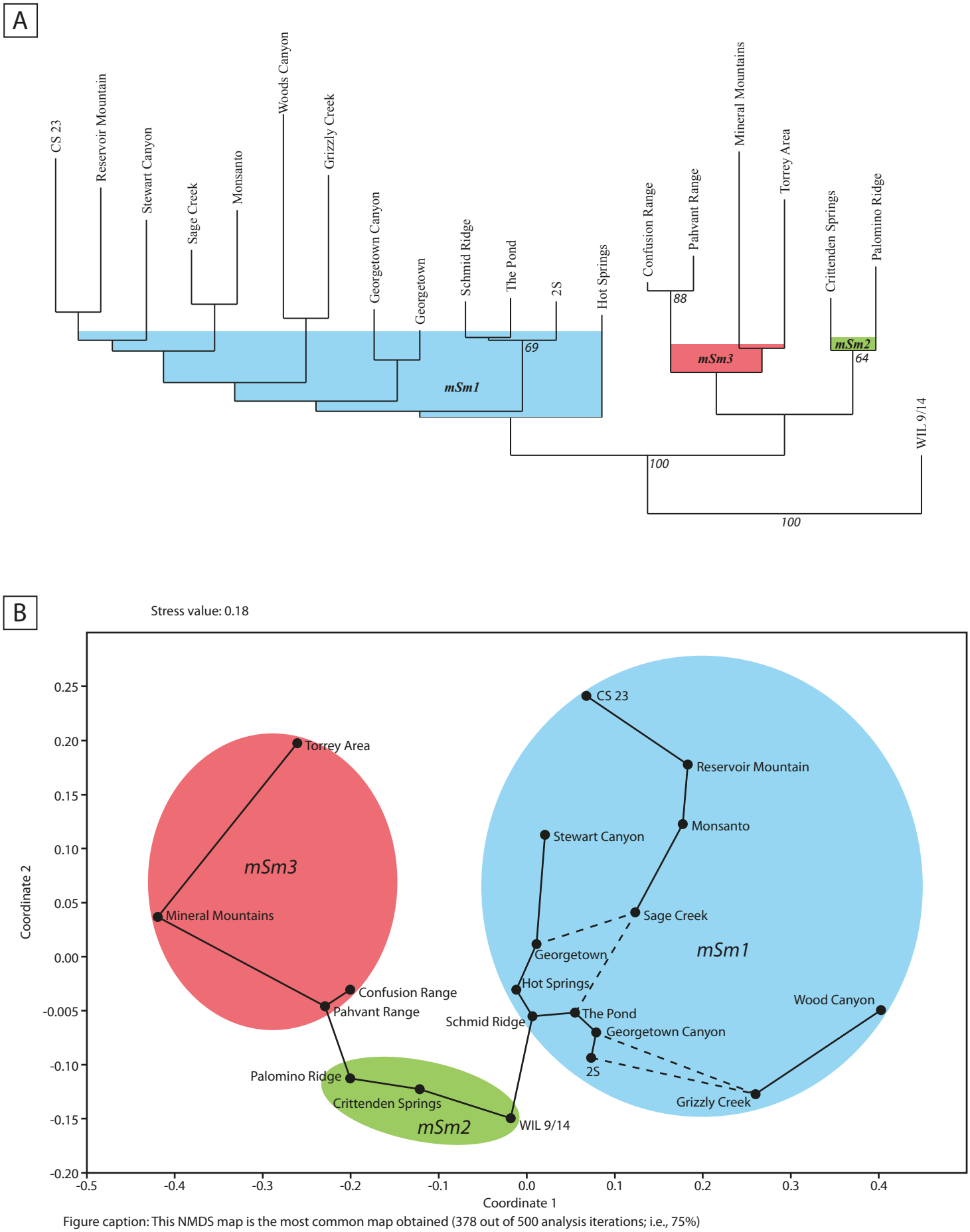

Figure caption: This NMDS map is the most common map obtained (378 out of 500 analysis iterations; i.e., 75%) and it is the one with the lowest stress value (0.184).

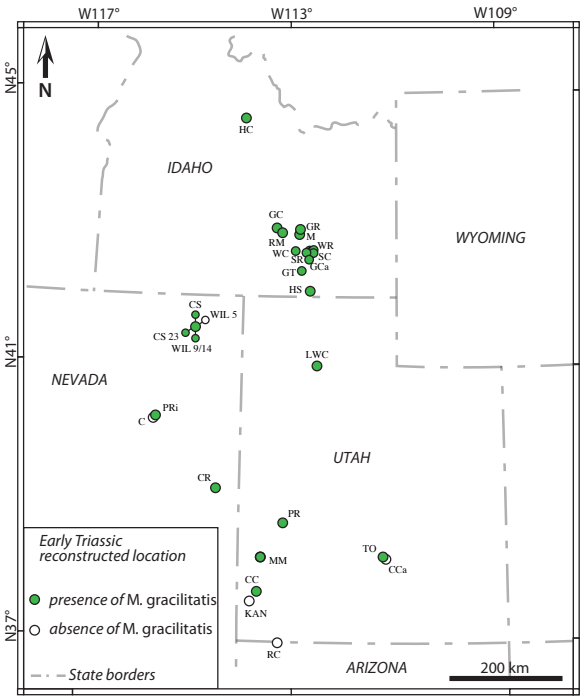
W117°
W113°
W109°
N45°
N41°
N37°
N
IDAHO
WYOMING
NEVADA
UTAH
ARIZONA
HC
GC
GR
M
RM
WC
WR
SR
SC
GT
GCa
HS
CS
WIL 5
CS 23
WIL 9/14
LWC
PRi
C
CR
PR
MM
TO
CCa
CC
KAN
RC
Early Triassic reconstructed location
presence of M. gracilitatis
absence of M. gracilitatis
State borders
200 km

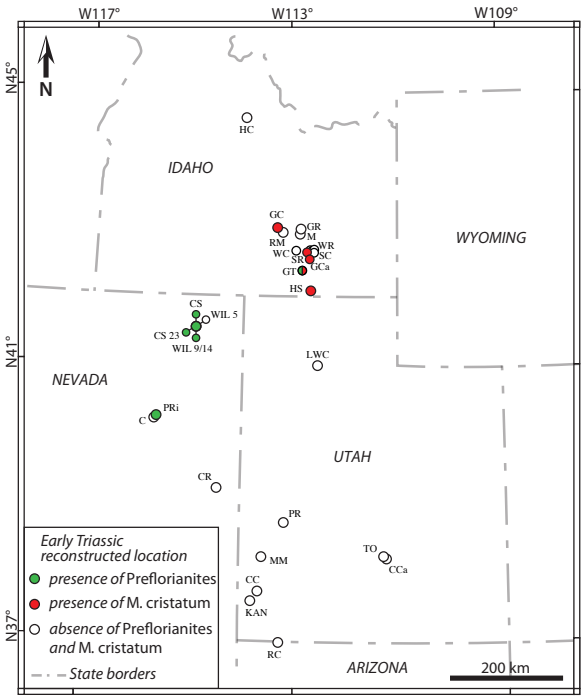
W117°
W113°
W109°
N45°
N41°
N37°
N
IDAHO
WYOMING
NEVADA
UTAH
ARIZONA
HC
GC
GR
M
RM
WC
WR
SR
SC
GT
GCa
HS
CS
WIL 5
CS 23
WIL 9/14
LWC
PRi
C
CR
PR
MM
TO
CCa
CC
KAN
RC
Early Triassic reconstructed location
presence of Preflorianites
presence of M. cristatum
absence of Preflorianites and M. cristatum
State borders
200 km

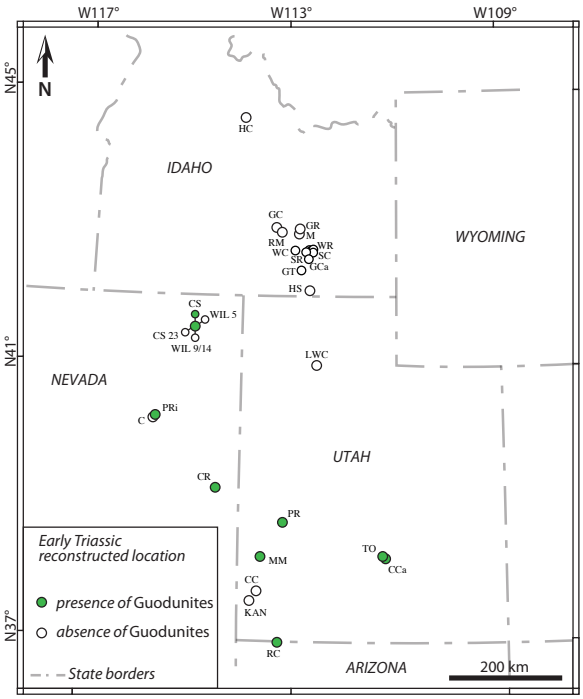
W117°
W113°
W109°
N45°
N41°
N37°
N
IDAHO
WYOMING
NEVADA
UTAH
ARIZONA
HC
GC
GR
M
RM
WC
WR
SR
SC
GT
GCa
HS
CS
WIL 5
CS 23
WIL 9/14
LWC
PRi
C
CR
PR
MM
TO
CCa
CC
KAN
RC
Early Triassic reconstructed location
presence of Guodunites
absence of Guodunites
State borders
200 km

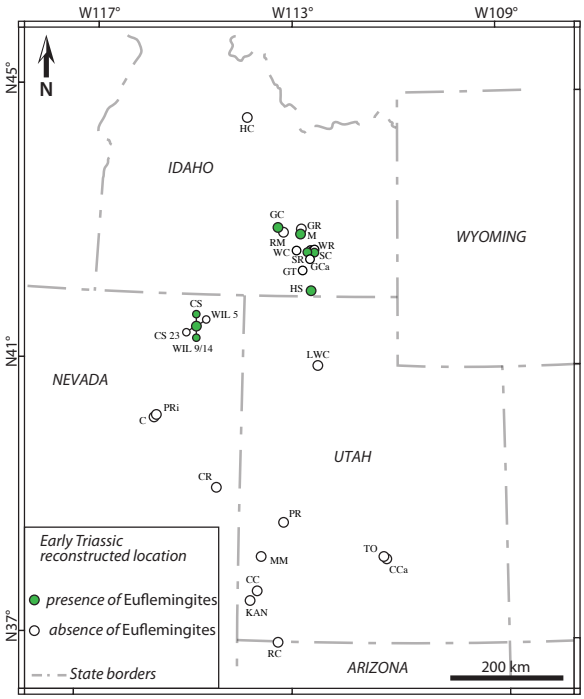
W117°
W113°
W109°
N45°
N41°
N37°
N
IDAHO
WYOMING
NEVADA
UTAH
ARIZONA
HC
GC
GR
M
RM
WC
WR
SR
SC
GT
GCa
HS
CS
WIL 5
CS 23
WIL 9/14
LWC
PRi
C
CR
PR
MM
TO
CCa
CC
KAN
RC
Early Triassic reconstructed location
presence of Euflemingites
absence of Euflemingites
State borders
200 km

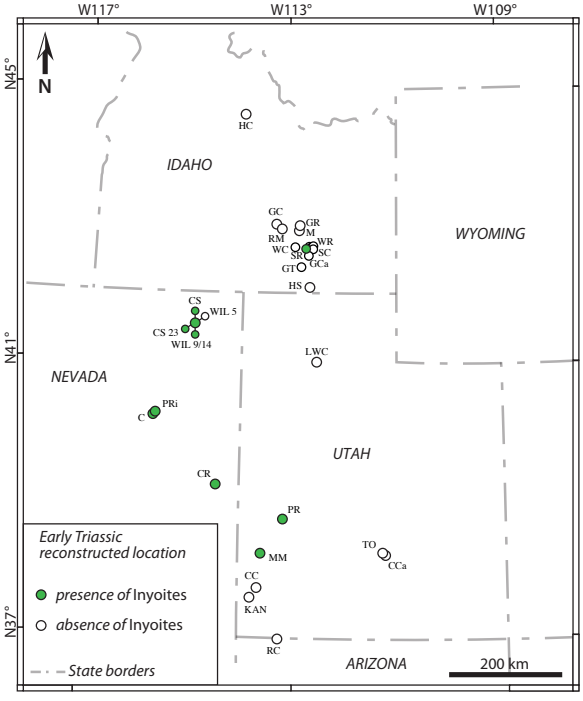
W117°
W113°
W109°
N45°
N41°
N37°
N
IDAHO
WYOMING
NEVADA
UTAH
ARIZONA
HC
GC
GR
M
RM
WC
WR
SR
SC
GT
GCa
HS
CS
WIL 5
CS 23
WIL 9/14
LWC
PRi
C
CR
PR
MM
TO
CCa
CC
KAN
RC
Early Triassic reconstructed location
presence of Inyoites
absence of Inyoites
State borders
200 km

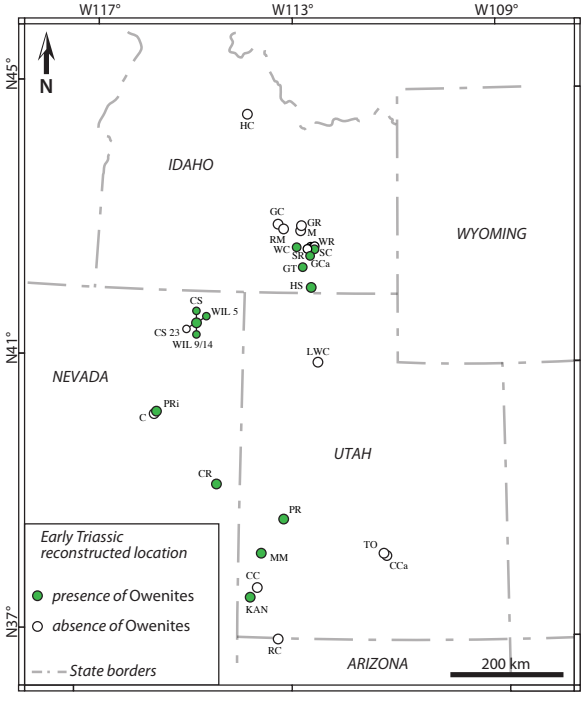
W117°
W113°
W109°
N45°
N41°
N37°
N
IDAHO
WYOMING
NEVADA
UTAH
ARIZONA
HC
GC
GR
M
RM
WC
WR
SR
SC
GT
GCa
HS
CS
WIL 5
CS 23
WIL 9/14
LWC
PRi
C
CR
PR
MM
TO
CCa
CC
KAN
RC
Early Triassic reconstructed location
presence of Owenites
absence of Owenites
State borders
200 km

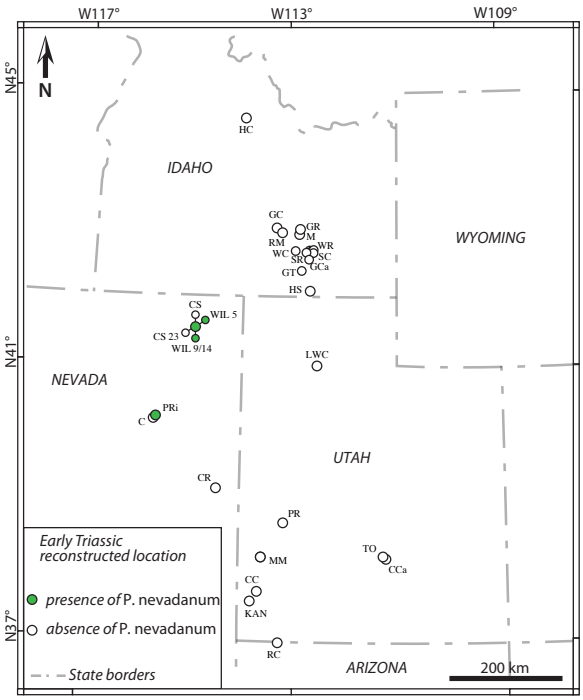
W117°
W113°
W109°
N45°
N41°
N37°
N
IDAHO
WYOMING
NEVADA
UTAH
ARIZONA
HC
GC
GR
M
RM
WR
WC
SC
SR
GCa
GT
HS
CS
WIL 5
CS 23
WIL 9/14
LWC
PRi
C
CR
PR
MM
TO
CCa
CC
KAN
RC
Early Triassic reconstructed location
presence of P. nevadanum
absence of P. nevadanum
State borders
200 km

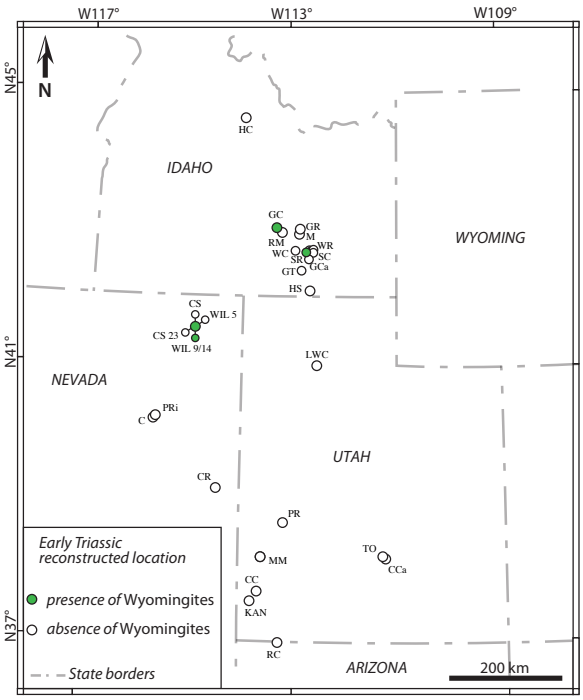
W117°
W113°
W109°
N45°
N41°
N37°
N
IDAHO
WYOMING
NEVADA
UTAH
ARIZONA
HC
GC
GR
M
RM
WR
WC
SC
SR
GCa
GT
HS
CS
WIL 5
CS 23
WIL 9/14
LWC
PRi
C
CR
PR
MM
TO
CCa
CC
KAN
RC
Early Triassic reconstructed location
presence of Wyomingites
absence of Wyomingites
State borders
200 km

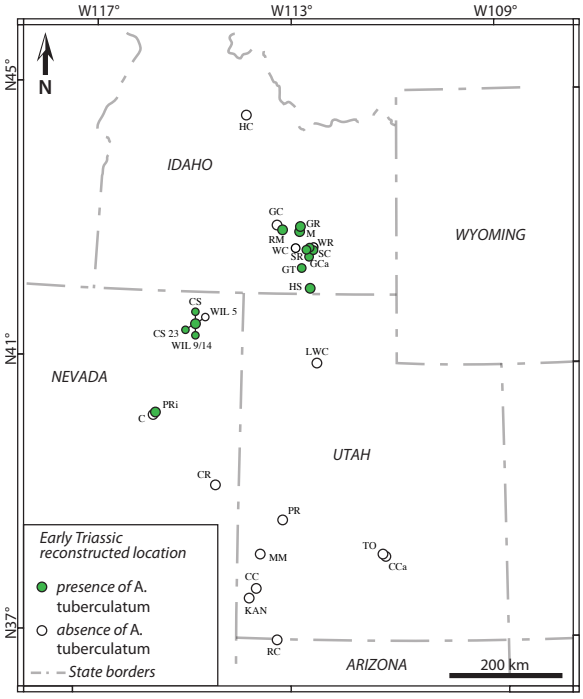
W117°
W113°
W109°
N45°
N41°
N37°
N
IDAHO
WYOMING
NEVADA
UTAH
ARIZONA
HC
GC
GR
M
RM
WR
WC
SC
SR
GCa
GT
HS
CS
WIL 5
CS 23
WIL 9/14
LWC
PRi
C
CR
PR
MM
TO
CCa
CC
KAN
RC
Early Triassic reconstructed location
presence of A. tuberculatum
absence of A. tuberculatum
State borders
200 km

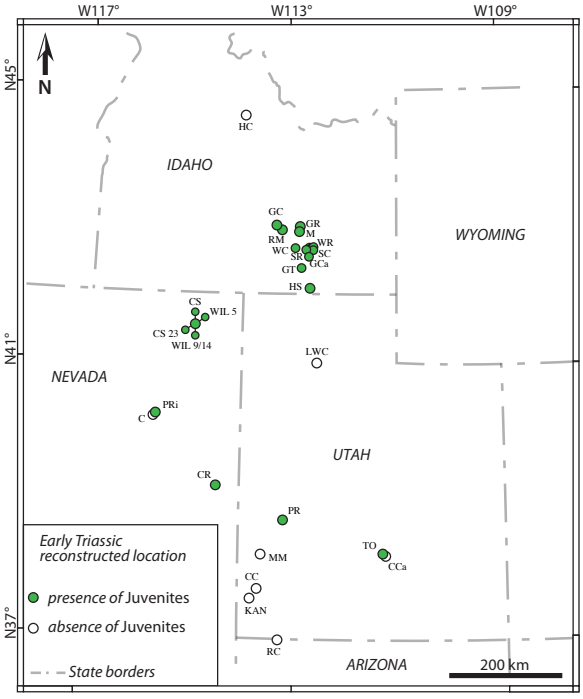
W117°
W113°
W109°
N45°
N41°
N37°
N
IDAHO
WYOMING
NEVADA
UTAH
ARIZONA
HC
GC
GR
M
RM
WR
WC
SC
SR
GCa
GT
HS
CS
WIL 5
CS 23
WIL 9/14
LWC
PRi
C
CR
PR
MM
TO
CCa
CC
KAN
RC
Early Triassic reconstructed location
presence of Juvenites
absence of Juvenites
State borders
200 km

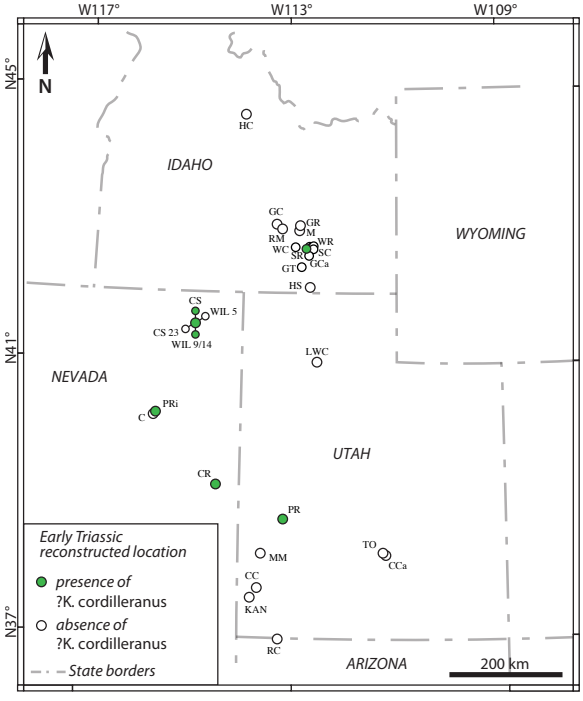
W117°
W113°
W109°
N45°
N41°
N37°
N
IDAHO
WYOMING
NEVADA
UTAH
ARIZONA
HC
GC
GR
M
RM
WR
WC
SC
SR
GCa
GT
HS
CS
WIL 5
CS 23
WIL 9/14
LWC
PRi
C
CR
PR
MM
TO
CCa
CC
KAN
RC
Early Triassic reconstructed location
presence of ?K. cordilleranus
absence of ?K. cordilleranus
State borders
200 km

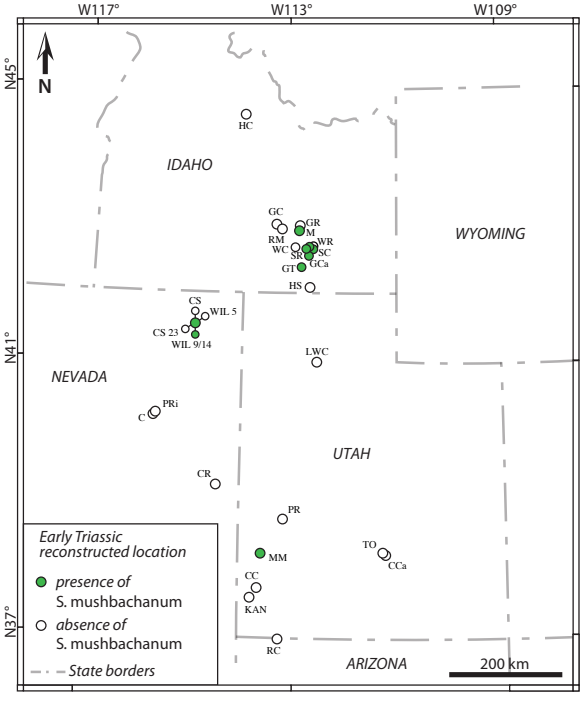
W117°
W113°
W109°
N45°
N41°
N37°
N
IDAHO
WYOMING
NEVADA
UTAH
ARIZONA
HC
GC
GR
M
RM
WR
WC
SC
SR
GCa
GT
HS
CS
WIL 5
CS 23
WIL 9/14
LWC
PRi
C
CR
PR
MM
TO
CCa
CC
KAN
RC
Early Triassic reconstructed location
presence of S. mushbachanum
absence of S. mushbachanum
State borders
200 km

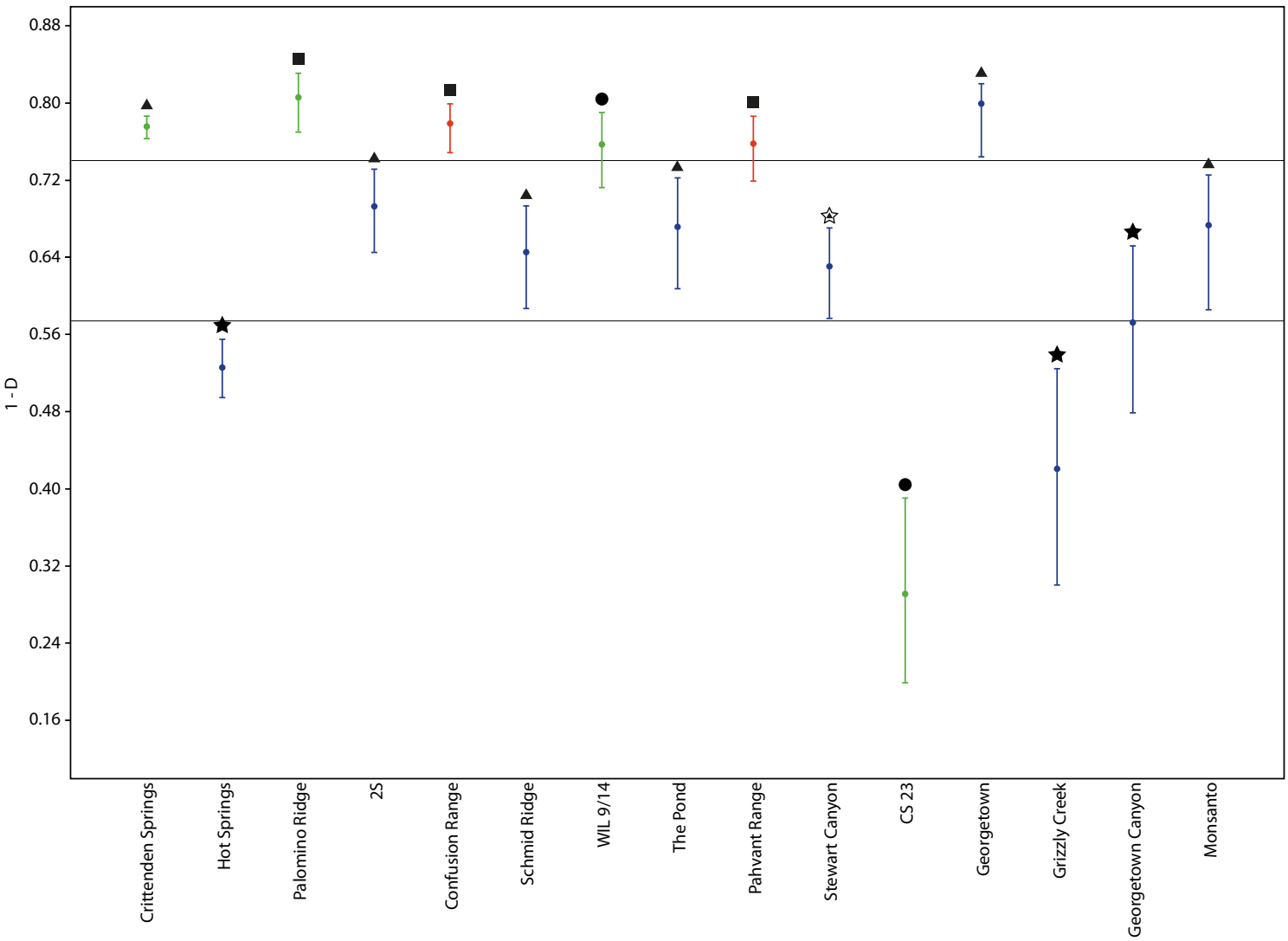
0.88
0.80
0.72
0.64
0.56
0.48
0.40
0.32
0.24
0.16
1 - D
Crittenden Springs
Hot Springs
Palomino Ridge
2S
Confusion Range
Schmid Ridge
WIL 9/14
The Pond
Pahvant Range
Stewart Canyon
CS 23
Georgetown
Grizzly Creek
Georgetown Canyon
Monsanto

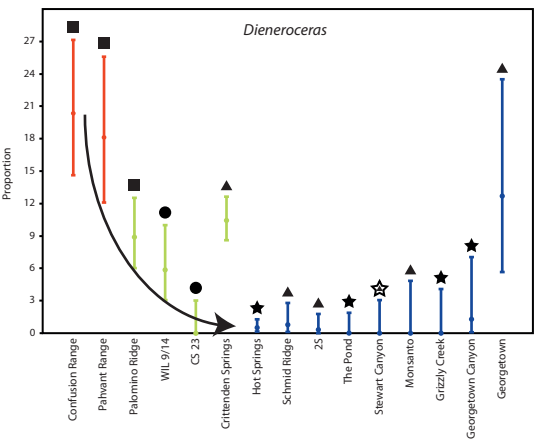
Dieneroceras
Proportion
0
3
6
9
12
15
18
21
24
27
Confusion Range
Palvant Range
Palomino Ridge
WIL 9/14
CS 23
Crittenden Springs
Hot Springs
Schmid Ridge
2S
The Pond
Stewart Canyon
Monsanto
Grizzly Creek
Georgetown Canyon
Georgetown

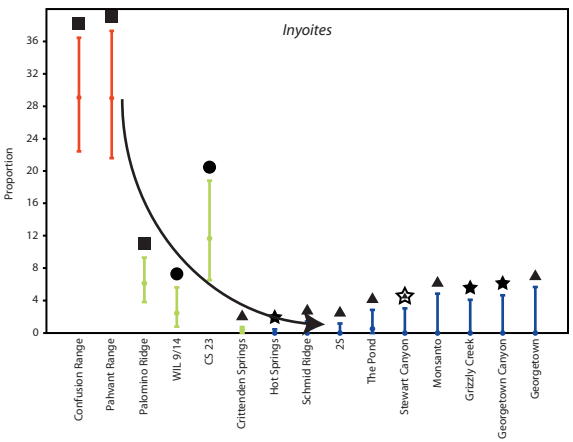
Inyoites
Proportion
0
4
8
12
16
20
24
28
32
36
Confusion Range
Palvant Range
Palomino Ridge
WIL 9/14
CS 23
Crittenden Springs
Hot Springs
Schmid Ridge
2S
The Pond
Stewart Canyon
Monsanto
Grizzly Creek
Georgetown Canyon
Georgetown

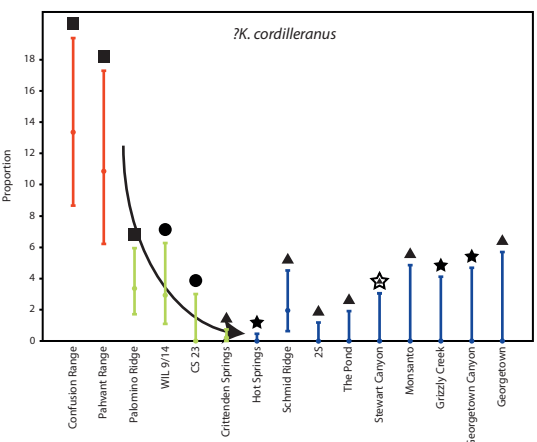
?K. cordilleranus
Proportion
0
2
4
6
8
10
12
14
16
18
Confusion Range
Palvant Range
Palomino Ridge
WIL 9/14
CS 23
Crittenden Springs
Hot Springs
Schmid Ridge
2S
The Pond
Stewart Canyon
Monsanto
Grizzly Creek
Georgetown Canyon
Georgetown

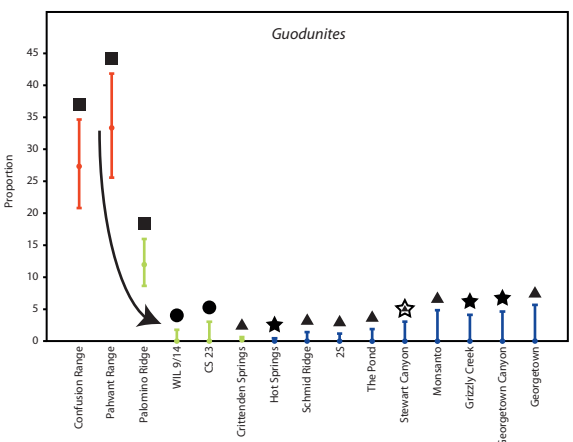
Guodunites
Proportion
0
5
10
15
20
25
30
35
40
45
Confusion Range
Palvant Range
Palomino Ridge
WIL 9/14
CS 23
Crittenden Springs
Hot Springs
Schmid Ridge
2S
The Pond
Stewart Canyon
Monsanto
Grizzly Creek
Georgetown Canyon
Georgetown

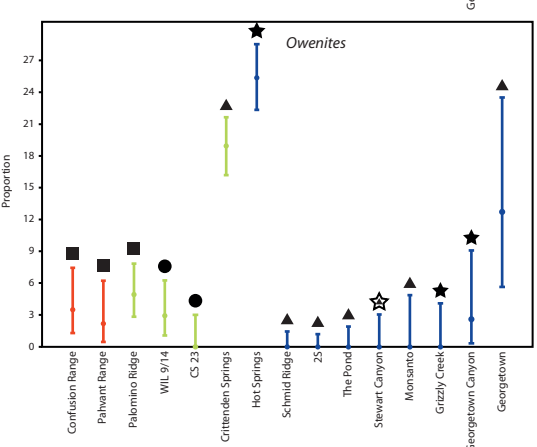
Owenites
Proportion
0
3
6
9
12
15
18
21
24
27
Confusion Range
Palvant Range
Palomino Ridge
WIL 9/14
CS 23
Crittenden Springs
Hot Springs
Schmid Ridge
2S
The Pond
Stewart Canyon
Monsanto
Grizzly Creek
Georgetown Canyon
Georgetown

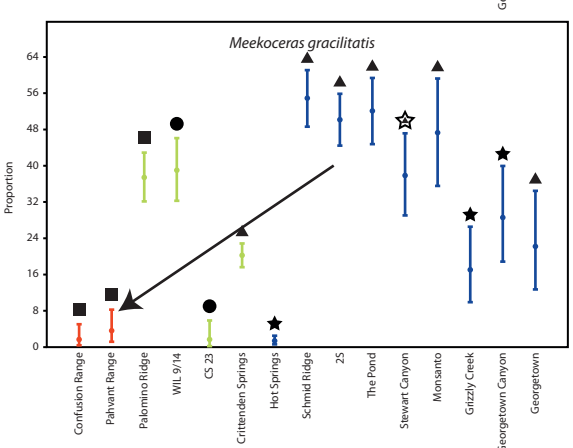
Meekoceras gracilitatis
Proportion
0
8
16
24
32
40
48
56
64
Confusion Range
Palvant Range
Palomino Ridge
WIL 9/14
CS 23
Crittenden Springs
Hot Springs
Schmid Ridge
2S
The Pond
Stewart Canyon
Monsanto
Grizzly Creek
Georgetown Canyon
Georgetown

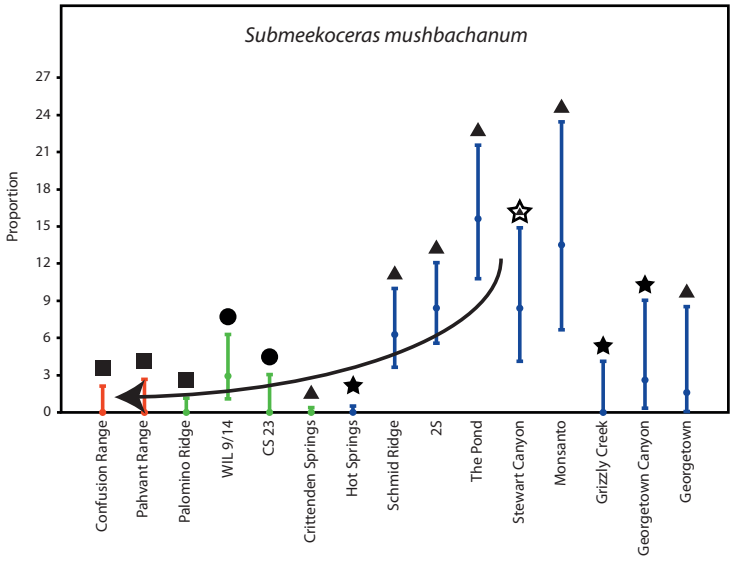
Submeekoceras mushbachanum
Proportion
0
3
6
9
12
15
18
21
24
27
Confusion Range
Pahvant Range
Palomino Ridge
WIL 9/14
CS 23
Crittenden Springs
Hot Springs
Schmid Ridge
2S
The Pond
Stewart Canyon
Monsanto
Grizzly Creek
Georgetown Canyon
Georgetown

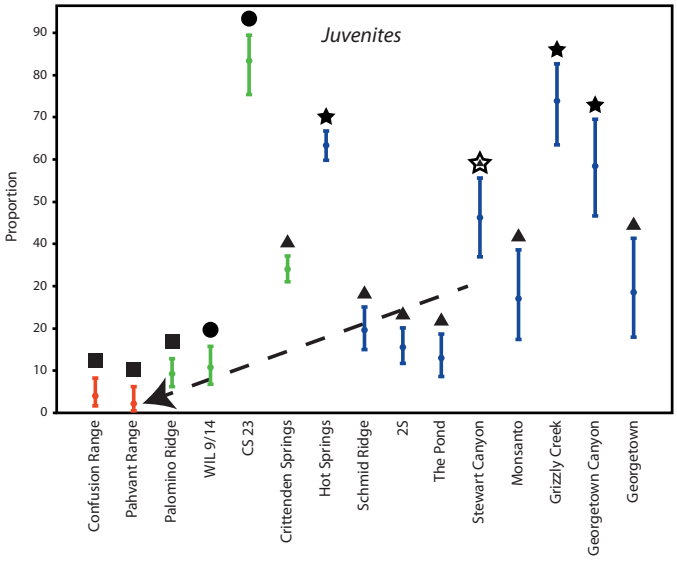
Juvenites
Proportion
0
10
20
30
40
50
60
70
80
90
Confusion Range
Pahvant Range
Palomino Ridge
WIL 9/14
CS 23
Crittenden Springs
Hot Springs
Schmid Ridge
2S
The Pond
Stewart Canyon
Monsanto
Grizzly Creek
Georgetown Canyon
Georgetown

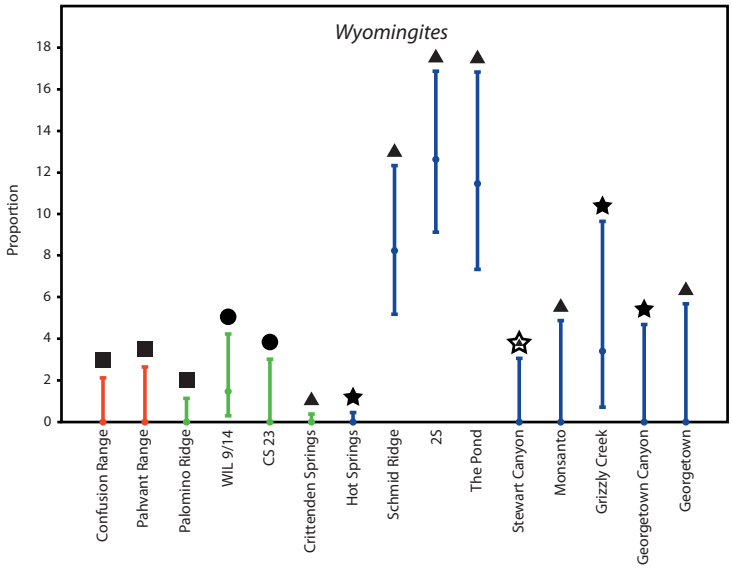
Wyomingites
Proportion
0
2
4
6
8
10
12
14
16
18
Confusion Range
Pahvant Range
Palomino Ridge
WIL 9/14
CS 23
Crittenden Springs
Hot Springs
Schmid Ridge
2S
The Pond
Stewart Canyon
Monsanto
Grizzly Creek
Georgetown Canyon
Georgetown

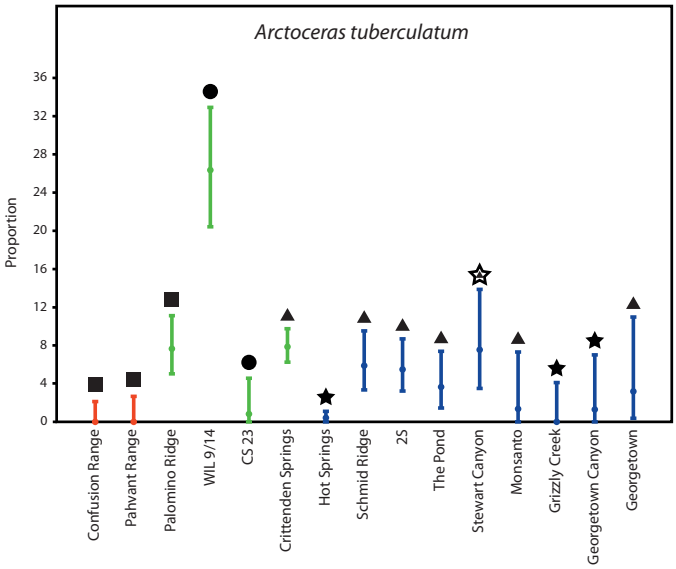
Arctoceras tuberculatum
Proportion
0
4
8
12
16
20
24
28
32
36
Confusion Range
Pahvant Range
Palomino Ridge
WIL 9/14
CS 23
Crittenden Springs
Hot Springs
Schmid Ridge
2S
The Pond
Stewart Canyon
Monsanto
Grizzly Creek
Georgetown Canyon
Georgetown

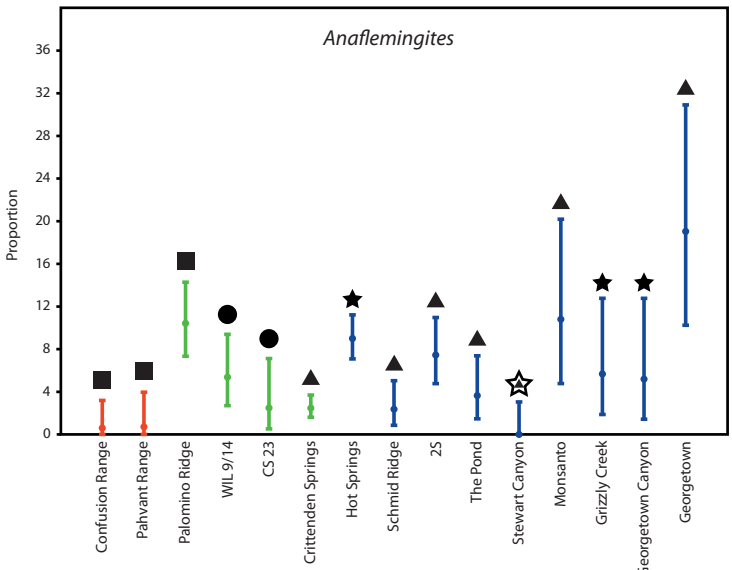
Anaflemingites
Proportion
0
4
8
12
16
20
24
28
32
36
Confusion Range
Pahvant Range
Palomino Ridge
WIL 9/14
CS 23
Crittenden Springs
Hot Springs
Schmid Ridge
2S
The Pond
Stewart Canyon
Monsanto
Grizzly Creek
Georgetown Canyon
Georgetown

middle Smithian	*Guodunites monneti*	*Guodunites hooveri*	*Churkites noblei*	*Lanceolites compactus*	*Lanceolites bicarinatus*	*Invoites oweni*	*Owenites koeneni*	*Meekoceras gracilitatis*	*Meekoceras cristatum*	*Hedenstroemia kossmati*	*Preflorianites toulai*	*Preflorianites radians*	*Aspenites acutus*	*Anaflemingites cf. silberlingi*	*Anaflemingites russelli*	*?Kashmirites cordilleranus*	*Palominoceras nevadanum*
Confusion Range	1	1	1	1	1	1	1	1	0	1	0	0	1	0	0	1	0
Pahvant Range	1	1	1	1	1	1	1	1	0	1	0	0	0	0	0	1	0
Mineral Mountains	0	1	1	0	0	1	0	1	0	0	0	0	0	0	0	0	0
Torrey Area	0	1	1	1	0	0	0	1	0	1	0	0	0	0	0	0	0
Crittenden Springs	1	0	1	1	0	1	1	1	0	1	0	1	1	0	0	1	0
CS 23	0	0	0	1	1	1	0	1	0	0	1	0	1	0	1	0	0
Palomino Ridge	1	1	1	1	0	1	1	1	0	1	1	0	1	1	0	1	1
WIL 9/14	0	0	1	0	0	1	1	1	0	0	1	1	1	0	1	1	1
Wood Canyon	0	0	0	0	0	0	1	1	0	0	0	0	0	0	1	0	0
Grizzly Creek	0	0	0	0	0	0	0	1	1	0	0	0	1	0	1	0	0
Hot Springs	0	0	1	1	1	0	1	1	1	0	0	0	1	1	1	0	0
Schmid Ridge	0	0	1	1	1	0	0	1	1	1	0	0	1	0	1	1	0
2S	0	0	1	0	1	0	0	1	1	1	0	0	1	0	1	0	0
The Pond	0	0	1	1	1	0	0	1	1	1	0	0	1	0	1	0	0
Georgetown Canyon	0	0	1	0	0	0	1	1	1	0	0	0	1	0	1	0	0
Georgetown	0	0	1	1	0	0	1	1	0	0	0	0	1	0	1	0	0
Sage Creek	0	0	0	1	0	0	1	1	0	0	0	0	1	0	1	0	0
Reservoir Mountain	0	0	0	0	0	0	0	1	0	0	0	0	1	0	1	0	0
Monsanto	0	0	0	1	0	0	0	1	0	0	0	0	1	0	1	0	0
Stewart Canyon	0	0	0	1	1	0	0	1	0	0	0	0	1	0	0	0	0

	Parussuria compressa	*Dieneroceras dieneri*	*Dieneroceras knechti*	*"Dagnoceras"*	*Owenites carpenteri*	*Juvenites*	*Pseudaspidites silberlingi*	*Proharpoceras carinatitabulatum*	*Pseudosageceras multilobatum*	*Arctoceras tuberculatum*	*Submeekoceras mushbachanum*	*Flemingites*	*Euflemingites*	*Wyomingites*	*Paranannites aspenensis*	*Invoites sp.*
Confusion Range	1	1	0	0	1	1	0	0	1	0	0	0	0	0	0	0
Pahvant Range	1	1	0	0	1	1	0	0	1	0	0	1	0	0	0	0
Mineral Mountains	1	1	0	0	1	0	0	0	0	0	1	0	0	0	0	0
Torrey Area	1	0	0	0	0	1	0	0	0	0	0	0	0	0	0	0
Crittenden Springs	1	1	1	0	0	1	1	1	1	1	0	0	1	0	1	1
CS 23	0	0	0	0	0	1	0	0	0	1	0	0	0	0	0	1
Palomino Ridge	1	1	1	0	1	1	0	1	1	1	0	0	0	0	1	1
WIL 9/14	1	1	0	0	0	1	0	0	1	1	1	0	1	1	0	1
Wood Canyon	0	1	0	0	0	1	0	0	0	0	0	1	0	0	0	0
Grizzly Creek	0	0	0	0	0	1	0	0	1	0	0	1	1	1	0	0
Hot Springs	1	1	0	0	1	1	0	0	1	1	0	0	1	0	1	0
Schmid Ridge	1	1	0	1	0	1	1	0	1	1	1	0	1	1	1	0
2S	1	1	0	1	0	1	1	0	1	1	1	1	1	1	0	0
The Pond	1	0	0	1	0	1	1	0	1	1	1	1	1	1	1	1
Georgetown Canyon	1	1	0	0	0	1	1	0	1	1	1	1	0	0	0	0
Georgetown	1	1	0	0	0	1	1	0	1	1	1	0	0	0	0	0
Sage Creek	0	0	0	0	0	1	0	0	1	1	1	0	1	0	1	0
Reservoir Mountain	1	0	0	0	0	1	0	0	0	1	0	0	0	0	0	0
Monsanto	0	0	0	1	0	1	0	0	0	1	1	0	1	0	0	0
Stewart Canyon	1	0	0	0	0	1	1	0	1	1	1	0	0	0	0	0

Late Smithian	*Pseudosageceras augustum*	*Anasibirites kingianus*	*Anasibirites multiformis*	*Wasatchites perrini*	*Hemiprionites walcotti*	*Hemiprionites typus*	*Arctoprionites resseri*	*Prionitidae indet.*	*Xenoceltites subevolutus*
Confusion Range	0	0	1	1	1	1	0	0	1
Crittenden Springs	1	1	1	1	1	1	1	0	1
Palomino Ridge	1	1	1	1	1	1	1	1	1
Black Rock Canyon	0	1	1	1	1	1	1	0	0
Lower Weber Canyon	0	1	1	1	1	1	1	0	1
WIL 4	0	1	1	1	1	1	1	0	0
WIL 6	0	1	1	0	1	1	1	1	1

	Total nb. of specimens	*Meekoceras gracilitatis*	Total - *M. gracilitatis*	% *M. gracilitatis*	*Guadunites*	Total - *Guadunites*	% *Guadunites*	*Owenites*	Total - *Owenites*	% *Owenites*	*Anaflemingites*	Total - *Anaflemingites*	% *Anaflemingites*	*?K. cordilleranus*	Total - *?K. cordilleranus*	% *?Kashmirites cordilleranus*	*Juvenites*	Total - *Juvenites*	% *Juvenites*
Confusion Range	172	3	169	1.7	47	125	27.3	6	166	3.5	1	171	0.6	23	149	13.4	7	165	4.1
Pahvant Range	138	5	133	3.6	46	92	33.3	3	135	2.2	1	137	0.7	15	123	10.9	3	135	2.2
Palomino Ridge	326	122	204	37.4	39	287	12.0	16	310	4.9	34	292	10.4	11	315	3.4	30	296	9.2
WIL 9/14	205	80	125	39.0	0	205	0.0	6	199	2.9	11	194	5.4	6	199	2.9	22	183	10.7
CS 23	120	2	118	1.7	0	120	0.0	0	120	0.0	3	117	2.5	0	120	0.0	100	20	83.3
Crittenden Springs	968	175	793	18.1	1	967	0.1	162	806	16.7	24	944	2.5	2	966	0.2	329	639	34.0
Hot Springs	789	11	778	1.4	0	789	0.0	200	589	25.3	71	718	9.0	0	789	0.0	500	289	63.4
Schmid Ridge	255	140	115	54.9	0	255	0.0	0	255	0.0	6	249	2.4	5	250	2.0	50	205	19.6
2S	309	155	154	50.2	0	309	0.0	0	309	0.0	23	286	7.4	0	309	0.0	48	261	15.5
The Pond	192	100	92	52.1	0	192	0.0	0	192	0.0	7	185	3.6	0	192	0.0	25	167	13.0
Stewart Canyon	119	45	74	37.8	0	119	0.0	0	119	0.0	0	119	0.0	0	119	0.0	55	64	46.2
Monsanto	74	35	39	47.3	0	74	0.0	0	74	0.0	8	66	10.8	0	74	0.0	20	54	27.0
Grizzly Creek	88	15	73	17.0	0	88	0.0	0	88	0.0	5	83	5.7	0	88	0.0	65	23	73.9
Georgetown Canyon	77	22	55	28.6	0	77	0.0	2	75	2.6	4	73	5.2	0	77	0.0	45	32	58.4
Georgetown	63	14	49	22.2	0	63	0.0	8	55	12.7	12	51	19.0	0	63	0.0	18	45	28.6
Chi-2 test result		$chi^2 = 784.5$; $p = 2\times10^{-158}$			$chi^2 = 858.1$; $p = 4\times10^{-174}$			$chi^2 = 414.1$; $p = 1\times10^{-79}$			$chi^2 = 110.5$; $p = 4\times10^{-17}$			$chi^2 = 278.9$; $p = 3\times10^{-51}$			$chi^2 = 906.9$; $p = 1\times10^{-184}$		

	Wyomingites	Total - *Wyomingites*	% *Wyomingites*	*Arctoceras*	Total - *Arctoceras*	% *Arctoceras*	*Inyoites*	Total - *Inyoites*	% *Inyoites*	*Dieneroceras*	Total - *Dieneroceras*	% *Dieneroceras*	*Submeekoceras mushbachanum*	Total - *S. mushbachanum*	% *Submeekoceras mushbachanum*
Confusion Range	0	172	0.0	0	172	0.0	50	122	29.1	35	137	20.3	0	172	0.0
Pahvant Range	0	138	0.0	0	138	0.0	40	98	29.0	25	113	18.1	0	138	0.0
Palomino Ridge	0	326	0.0	25	301	7.7	20	306	6.1	29	297	8.9	0	326	0.0
WIL 9/14	3	202	1.5	54	151	26.3	5	200	2.4	12	193	5.9	6	199	2.9
CS 23	0	120	0.0	1	119	0.8	14	106	11.7	0	120	0.0	0	120	0.0
Crittenden Springs	0	968	0.0	76	892	7.9	2	966	0.2	197	771	20.4	0	968	0.0
Hot Springs	0	789	0.0	3	786	0.4	0	789	0.0	4	785	0.5	0	789	0.0
Schmid Ridge	21	234	8.2	15	240	5.9	0	255	0.0	2	253	0.8	16	239	6.3
2S	39	270	12.6	17	292	5.5	0	309	0.0	1	308	0.3	26	283	8.4
The Pond	22	170	11.5	7	185	3.6	1	191	0.5	0	192	0.0	30	162	15.6
Stewart Canyon	0	119	0.0	9	110	7.6	0	119	0.0	0	119	0.0	10	109	8.4
Monsanto	0	74	0.0	1	73	1.4	0	74	0.0	0	74	0.0	10	64	13.5
Grizzly Creek	3	85	3.4	0	88	0.0	0	88	0.0	0	88	0.0	0	88	0.0
Georgetown Canyon	0	77	0.0	1	76	1.3	0	77	0.0	1	76	1.3	2	75	2.6
Georgetown	0	63	0.0	2	61	3.2	0	63	0.0	8	55	12.7	1	62	1.6
Chi-2 test result		$chi^2 = 332.0$; $p = 2\times10^{-62}$			$chi^2 = 264.3$; $p = 3\times10^{-48}$			$chi^2 = 752.8$; $p = 1\times10^{-151}$			$chi^2 = 415.3$; $p = 8\times10^{-80}$			$chi^2 = 304.7$; $p = 1\times10^{-54}$	

Total = total de spécimens pour la liste d'espèces sélectionnées

Main facies associations	Biota	Other components	Sedimentary structures	Preservation	Depositional environments	Basin position
A Ammonoid-rich floatstones in a mud-to wackestone matrix	Ammonoids, thin-shell bivalves, gastropods and echinoderms	siltites (fine to very fine subrounded quartz) organized in mm-thick layers	Planar laminations, storm-induced deposits (HCS and bioaccumulations with erosional base); Cm-thick siltites layers alternating with pluri-Cm and dm-thick bioclastic-rich layers	Complete and oriented ammonoids with poorly preserved and fragmented phragmocone and infilled by a micritic matrix; bivalves and gastropods reworked	Upper to lower Offshore with storm-induced deposits; mud dominated outer platform	Confusion Range, Pahvant Range and Palomino Ridge
B Altenance of ammonoid (1) in a peloidal wackestone to packstone matrix and bioclastic-rich (2) floatstones in a wackestone matrix	(1) Ammonoids, thin-shell bivalves and gastropods; (2) bivalves, gastropods and echinoderms	-	Storm-induced deposits with grading and erosion base (amalgamated storms composed of ammonoids and bivalves, respectively)	(1) Complete and oriented ammonoids with poorly preserved and fragmented phragmocone and infilled by a peloidal and microbial matrix; desarticulated thin bivalves and gastropods; (2) Desarticulated thin bivalves, broken thick bivalves and reworked gastropodes and bivalves (with dark micritic matrix)	Upper Offshore with amalgamated storm-induced deposits; mud dominated outer platform	CS23 and WIL9
C Ammonoid and bioclastic-rich floatstones in a mud-to wackestone matrix	Ammonoids, thick-shell bivalves, gastropods and echinoderms	-	Proximal storm-induced deposits (bioaccumulations with erosional base); Dm-thick bioaccumulations	Complete and oriented ammonoids with poorly preserved and fragmented phragmocone and infilled by a micritic matrix; bivalves and gastropods reworked	Upper Offshore (deep shoal domain); mid platform	Schmid Ridge, 2S, The Pond, Monsanto, Stewart Canyon, Georgetown and Crittenden Springs
D Bioclastic and ammonoid-rich (Juvenites) packstone	Thick-shell bivalves, ammonoids, serpulids, gastropods and ostracods	Very are clastics (quartz, phosphate and oxide grains)	Trough cross-bedding, planar to oblique laminations, bioturbations	Small and ball-shaped complete ammonoids infilled by a packstone matrix; fragments and micritized bivalves, gastropodes and other bioclasts	High energy subtidal shoals; inner platform	Hot Springs, Grizzly Creek, Stewart Canyon and Georgetown Canyon

	WIL 9/14	Palomino Ridge	Crittenden Springs
mSm1	43	55.66	48.76
mSm3	54.05	39.86	46.88

R \ *p*	mSm3	mSm2	mSm1	
mSm3		0.0583	0.0007	
mSm2	0.0583		0.052	
mSm1	0.0007	0.052	R = 0.54	

Taxon	Av. dissim	Contrib. %	Cumulative %	Mean South	Mean Inter	Mean North
Anaflemingites russelli	2.902	5.38	5.38	0	0.333	0.923
Guodunites hooveri	2.852	5.288	10.67	1	0.333	0
Inyoites oweni	2.649	4.912	15.58	0.75	1	0.0769
Arctoceras tuberculatum	2.382	4.416	20	0	1	0.846
Hedenstroemia kossmati	2.262	4.194	24.19	0.75	0.667	0.231
?Kashmirites cordilleranus	2.213	4.104	28.29	0.5	1	0.0769
Owenites carpenteri	2.099	3.891	32.18	0.75	0.333	0.0769
Churkites noblei	2.095	3.884	36.07	1	1	0.462
Aspenites acutus	2.035	3.773	39.84	0.25	1	0.923
Owenites koeneni	1.985	3.68	43.52	0.5	1	0.385
Submeekoceras mushbachanum	1.95	3.615	47.14	0.25	0.333	0.615
Dieneroceras dieneri	1.939	3.595	50.73	0.75	1	0.462
Euflemingites	1.915	3.551	54.28	0	0.667	0.538
Guodunites monneti	1.841	3.413	57.7	0.5	0.667	0
Pseudosageceras multilobatum	1.758	3.259	60.95	0.5	1	0.692
Lanceolites compactus	1.744	3.234	64.19	0.75	0.667	0.615
Lanceolites bicarinatus	1.694	3.141	67.33	0.5	0	0.462
Inyoites sp. indet.	1.662	3.081	70.41	0	1	0.154
Pseudaspidites silberlingi	1.55	2.874	73.29	0	0.333	0.462
Parussuria compressa	1.474	2.733	76.02	1	1	0.615
Flemingites sp. indet.	1.467	2.72	78.74	0.25	0	0.385
Paranannites aspenensis	1.451	2.691	81.43	0	0.667	0.308
Meekoceras cristatum	1.346	2.495	83.92	0	0	0.462
Wyomingites	1.209	2.241	86.17	0	0.333	0.308
Preflorianites toulai	1.167	2.163	88.33	0	0.667	0.0769
Preflorianites cf. radians	1.042	1.932	90.26	0	0.667	0
Palominoceras nevadanum	1.013	1.877	92.14	0	0.667	0
Proharpoceras carinatitabulatum	0.9792	1.815	93.95	0	0.667	0
Dieneroceras knechti	0.9792	1.815	95.77	0	0.667	0
Dagnoceras	0.8924	1.654	97.42	0	0	0.308
Juvenites	0.7485	1.388	98.81	0.75	1	1
Anaflemingites cf. silberlingi	0.6412	1.189	100	0	0.333	0.0769
Meekoceras gracilitatis	0	0	100	1	1	1

R = 0.35, P = 0.014	A	B	C	D
A	-	0.1991	0.0335	0.0263
B	0.1991	-	0.464	0.4751
C	0.0335	0.464	-	0.1957
D	0.0263	0.4751	0.1957	-

Taxon	Av. dissim	Contrib. %	Cumulative %	Mean A	Mean C	Mean B	Mean D
Juvenites	18.12	25.91	25.91	13.3	81.7	61	166
Meekoceras	15.77	22.55	48.46	43.3	103	41	23.3
Dienerocera	5.642	8.067	56.53	29.7	34.7	6	1.25
Guodunites	5.436	7.773	64.3	44	0.167	0	0
Inyoites	5.271	7.538	71.84	36.7	0.5	9.5	0
Owenites	5.133	7.339	79.18	8.33	28.3	3	50.5
A. tuberculat	4.173	5.968	85.14	8.33	19.7	27.5	3.25
Anaflemingit	3.249	4.646	89.79	12	13.3	7	20
S. mushbach	2.644	3.78	93.57	0	13.8	3	3
Wyomingites	2.279	3.259	96.83	0	13.7	1.5	0.75
?Kashmirites	2.217	3.17	100	16.3	1.17	3	0